Acoustic inverse scattering using topological derivative of far-field measurements-based L^2 cost functionals

Acoustic inverse scattering using topological derivative of far-field measurements-based L^2 cost functionals

Cédric Bellis[1]**, Marc Bonnet**[2] **and Fioralba Cakoni**[3]

[1] Department of Applied Physics and Applied Mathematics, Columbia University, New York, NY, USA
[2] POems (UMR 7231 CNRS-INRIA-ENSTA), ENSTA, Palaiseau, France
[3] Department of Mathematical Sciences, University of Delaware, Newark, NJ, USA

E-mail: bellis@lma.cnrs-mrs.fr, mbonnet@ensta.fr and cakoni@math.udel.edu

Abstract

Originally formulated in the context of topology optimization, the concept of topological derivative has also proved effective as a qualitative inversion tool for a wave-based identification of finite-sized objects. This approach remains, however, largely based on a heuristic interpretation of the topological derivative, whereas most other qualitative approaches to inverse scattering are backed by a mathematical justification. As an effort toward bridging this gap, this study focuses on a topological derivative approach applied to the L^2-norm of the misfit between far-field measurements. Either an inhomogeneous medium or a finite number of point-like scatterers are considered, using either the Born approximation or a full-scattering model. Topological derivative-based imaging functionals are analyzed using a suitable factorization of the far-field operator, for each of the considered cases, in order to characterize their behavior and assess their ability to reconstruct the unknown scatterer(s). Results include the justification of the usual sign heuristic underpinning the method for (i) the Born approximation and (ii) full-scattering models limited to moderately strong scatterers. Semi-analytical and numerical examples are presented. Within the chosen framework, the topological derivative approach is finally discussed and compared to other well-known qualitative methods.

1. Introduction

Inverse scattering has been the subject of intense studies over the last twenty years, and has in particular spawned the growth and flourishing of qualitative, sampling-based methods [1–3] that aim at providing a robust and computationally effective alternative to more customary approaches based on successive linearizations or iterative optimization methods. Since the *scattering operator* (see e.g. [4]) plays a central role in forward scattering problems, inverse scattering methods have early been designed as strategies to extract the information contained

in the corresponding *measurement operator* [5, 1]. The following brief bibliographical review on the subject highlights the importance of this idea and connections between some of these methods.

- Exploitation of the spectrum of the measurement or the scattering operator [6–8].
- Linear sampling and factorization methods, seen as two comparable strategies [9] to extract the information from the scattering operator in a 'simple' way [2, 10].
- Parallels between the MUSIC algorithm, linear sampling and factorization methods [10–12].
- Use of the MUSIC algorithm to deal with inverse scattering problems [13, 14].
- MUSIC algorithm and time reversal [13, 15].
- Time reversal and imaging [16–19].
- Exploitation of the spectrum of the time-reversal operator and DORT method (French acronym for *decomposition of the time-reversal operator*) [20–22].

In addition to all the aforementioned approaches, the concept of *topological derivative*, which first appeared in the context of topological optimization of structures [23, 24], revolves around the quantification of the leading perturbation of a given cost functional, namely its topological derivative, due to the creation of a virtual object of vanishingly small characteristic size at a prescribed location z inside the background (i.e. defect-free) medium. Over the last few years, the topological derivative of data misfit cost functionals has been investigated in a variety of inverse scattering situations as a way to define an indicator function of the hidden objects; see e.g. [25–32]. While defining and formulating the topological derivative of a given cost functional is mathematically rigorous, its subsequent use for imaging a given domain remains largely heuristic. Nonetheless, the method has been shown to lead to efficient and robust imaging functionals; moreover, it is very flexible in terms of exploitable data and misfit functionals, and easily implementable using classical computational methods [25–28, 32]. On the other hand, investigations toward a better theoretical understanding of this approach have begun only recently. For example, [28] points out the analogy with time reversal, and the imaging of a single small scatterer is mathematically studied in [29], where proofs of stability with respect to medium or measurement noises are also given.

This paper focuses on indicator functions provided by the topological derivative of L^2 misfit cost functionals, in the context of inverse scattering by an acoustic medium characterized by an inhomogeneous refraction index n. The available data are assumed to consist of measurements of the scattered far-field patterns, gathered into the far-field operator F. This work aims at providing a mathematical basis to the, until now heuristic, use of the topological derivative approach in this context. The behavior of the indicator function will be studied depending on the location of the sampling point z, the choice of the trial refraction index featured in the asymptotic analysis of the cost functional and the values of characteristic frequency, contrast $q = n^2 - 1$ and obstacle size. Scattering by either spatially extended inhomogeneities or a collection of point-like scatterers will be considered, either under the weak-scatterer (Born) approximation or using a full-scattering model taking into account multiple-scattering effects. In the latter case, a full justification of the topological derivative approach will be obtained only within limitations on the frequency and scatterer characteristics. The analysis, and the justification results obtained, exploits a fundamental relation, established here, between the topological derivative and the far-field operator F. In conjunction with the use of explicit factorizations of F in the different situations considered, this relation is instrumental in gaining insight into the workings of the topological derivative approach and putting it in perspective within the general class of sampling methodologies for inverse scattering, which are the two main objectives of this work.

2

This paper is accordingly organized as follows. Section 2 gathers background material on the forward scattering problem. Section 3 is then devoted to the topological derivative of far-field measurement-based least-squares cost functionals. Its validity as an indicator function is first justified under the Born approximation, and then partially extended to the full-scattering model, mainly by using connections with the far-field operator and exploiting its known factorization. The section ends with analytical and numerical examples. Similar analyses are next carried out in section 4 for the identification of spatially small, point-like obstacles (with full scattering modeled using the Foldy–Lax approximation), and again completed by numerical results. Finally, section 5 puts the topological derivative approach in a broader perspective, by discussing both its specificities and its connections with other sampling methods.

2. Forward acoustic scattering problem

Consider an infinite homogeneous background acoustic medium, occupying all of $\mathbb{R}^d$ with $d = 2$ or 3 and characterized by the constant wave velocity c_0. Let $D = \bigcup_{m=1}^{M} D_m \subset \mathbb{R}^d$ be an open and bounded domain with Lipschitz boundary ∂D and such that $\mathbb{R}^d \backslash \overline{D}$ is connected. D denotes the support of a scattering inhomogeneity characterized by a *real-valued* contrast function $q \in L^\infty(D)$, of constant sign in each connected component D_m, and for which there exists $n_D > 0$ such that $1 + q(x) \geqslant n_D^2$ for all $x \in D$. The contrast q is related to the index of refraction $n = c/c_0$ (with c denoting the wave velocity in D) by $q = n^2 - 1$. It is extended to $\mathbb{R}^d$ by setting $q = 0$, i.e. $n = 1$, in $\mathbb{R}^3 \setminus \overline{D}$.

Let $k = \omega/c_0$ be the wave number in the background medium. Considering an incident field u_i that is a known solution of the unperturbed Helmholtz equation $\Delta u + k^2 u = 0$ in $\mathbb{R}^d$, the forward acoustic scattering problem under consideration is

$$\Delta u + k^2(1 + q)u = 0 \quad \text{in } \mathbb{R}^d, \tag{1a}$$

$$u = u_i + v, \tag{1b}$$

$$\frac{\partial v}{\partial |x|} - \mathrm{i}kv = \mathcal{O}(|x|^{-(d+1)/2}) \quad \text{for } |x| \to \infty \tag{1c}$$

where $u \in H^1_{\text{loc}}(\mathbb{R}^d)$ is the total acoustic field, the scattered field v satisfies the Sommerfeld radiation condition (1c) uniformly in $\hat{x} = x/|x| \in \mathbb{S}$, with $\mathbb{S}$ denoting the unit circle if $d = 2$ or the unit sphere if $d = 3$. The latter condition implies the existence of a far-field pattern v^∞ such that

$$u(x) = u_i(x) + \gamma_d \frac{\mathrm{e}^{\mathrm{i}k|x|}}{|x|^{(d-1)/2}} v^\infty(\hat{x}) + \mathcal{O}(|x|^{-(d+1)/2}) \quad \text{for } |x| \to \infty, \tag{2}$$

where the parameter γ_d is such that

$$\gamma_2 = \mathrm{e}^{\mathrm{i}\pi/4}/\sqrt{8\pi k}, \qquad \gamma_3 = 1/4\pi.$$

The radiating fundamental solution Φ of the Helmholtz equation in $\mathbb{R}^d$ is given by

$$\Phi(x, y) = \frac{\mathrm{i}}{4} H_0^{(1)}(k|x - y|) \ \text{(for } d = 2), \qquad \Phi(x, y) = \frac{\mathrm{e}^{\mathrm{i}k|x-y|}}{4\pi|x - y|} \ \text{(for } d = 3),$$

where $H_0^{(1)}$ is the Hankel function of the first kind and order zero. Denoting by $h(\cdot, \theta)$, the plane wave propagating in the direction $\theta \in \mathbb{S}$ defined by

$$h(x, \theta) = \mathrm{e}^{\mathrm{i}kx \cdot \theta}, \qquad x \in \mathbb{R}^d, \tag{3}$$

3

the far-field pattern $\Phi_y^\infty(\hat{x})$ of Φ, such that the asymptotic expansion

$$\Phi(x, y) = \gamma_d \frac{e^{ik|x|}}{|x|^{(d-1)/2}} \Phi_y^\infty(\hat{x}) + \mathcal{O}(|x|^{-(d+1)/2}) \quad \text{for } |x| \to \infty \tag{4}$$

holds, is given by

$$\Phi_y^\infty(\hat{x}) = h(y, -\hat{x}) = \overline{h(y, \hat{x})}. \tag{5}$$

Solving problem (1*a*)–(1*c*) is known [5] to be equivalent to finding the solution $u \in L^2(D)$ of the Lippmann–Schwinger integral equation:

$$(I - ST_b)u = u_i, \tag{6}$$

where the volume potential operator $S : L^2(D) \to L^2(D)$ is defined by

$$S\varphi(x) := \int_D \varphi(y)\Phi(x, y)\,\mathrm{d}V_y, \qquad x \in D, \tag{7}$$

I is the identity, and the operator $T_b : L^2(D) \to L^2(D)$ is defined by $T_b\varphi = k^2 q\,\varphi$. Then, the scattered field v in $\mathbb{R}^d \setminus \bar{D}$ is given by the explicit integral representation

$$v(x) = ST_b u(x), \qquad x \in \mathbb{R}^d \setminus \bar{D}, \tag{8}$$

with S denoting the $L^2(D) \to H^1_{\mathrm{loc}}(\mathbb{R}^d)$ extension of the volume potential operator (7). In particular, using (2) and (4) in (8), the far-field pattern v^∞ is then given by

$$v^\infty(\hat{x}) = \int_D k^2 q(y) u(y) \overline{h(y, \hat{x})}\,\mathrm{d}V_y, \qquad \hat{x} \in \mathbb{S}. \tag{9}$$

The introduction of the parameter γ_d in definitions (2) and (4) of the far-field patterns makes the ensuing analysis and results independent, to a large extent, of the spatial dimension d.

If the incident field is chosen as a plane wave propagating in the direction $\theta \in \mathbb{S}$, i.e. $u_i = h(\cdot, \theta)$, the corresponding far-field pattern v^∞ is denoted $A(\cdot, \theta)$, i.e.:

$$u(x) = h(x, \theta) + \gamma_d \frac{e^{ik|x|}}{|x|^{(d-1)/2}} A(\hat{x}, \theta) + \mathcal{O}(|x|^{-(d+1)/2}) \quad \text{for } |x| \to \infty. \tag{10}$$

Then, if D is illuminated instead by a continuous superposition of plane waves, i.e. u_i is a Herglotz wave with density $g \in L^2(\mathbb{S})$:

$$u_i(x) = \int_\mathbb{S} h(x, \theta) g(\theta)\,\mathrm{d}S_\theta \quad x \in \mathbb{R}^d, \tag{11}$$

the corresponding far-field pattern v^∞ is expressed in terms of the far-field operator $F : L^2(\mathbb{S}) \to L^2(\mathbb{S})$ with kernel A:

$$v^\infty(\hat{x}) = Fg(\hat{x}), \qquad Fg(\hat{x}) := \int_\mathbb{S} A(\hat{x}, \theta) g(\theta)\,\mathrm{d}S_\theta, \tag{12}$$

which is known [10] to be normal (i.e. $FF^\star = F^\star F$) since q is real valued. Finally, the Herglotz operator H and its adjoint $H^\star$ are defined for later reference:

$$H : L^2(\mathbb{S}) \to L^2(D), \ Hg(x) = \int_\mathbb{S} h(x, \theta) g(\theta)\,\mathrm{d}S_\theta, \tag{13a}$$

$$H^\star : L^2(D) \to L^2(\mathbb{S}), \ H^\star\phi(\hat{x}) = \int_D h(y, -\hat{x})\phi(y)\,\mathrm{d}V_y = \int_D \overline{h(y, \hat{x})}\phi(y)\,\mathrm{d}V_y. \tag{13b}$$

The following identity satisfied by H will later prove very useful.

Lemma 1. *Let ζ_0 denote the function defined for $x \in \mathbb{R}^d$ by*

$$\zeta_0(x) = 2\pi J_0(k|x|) \ \ (d = 2), \quad \zeta_0(x) = 4\pi j_0(k|x|) = 4\pi \frac{\sin(k|x|)}{k|x|} \ \ (d = 3), \tag{14}$$

where J_0 is the Bessel function of the first kind and order zero and j_0 its spherical counterpart. Then, one has

$$H\Phi_z^\infty(y) = \zeta_0(y - z), \qquad y \in D.$$

Proof. By definition of H and Φ_z^∞, one has that

$$H\Phi_z^\infty(y) = \int_{\mathbb{S}} e^{ik(y-z)\cdot\theta} \, dS_\theta, \qquad y \in D.$$

The above integral is then readily seen to coincide (up to the appropriate constant factor) with the integral representation of the relevant Bessel function (see e.g. [33], formulas 10.9.1 and 10.54.1). $\qquad\square$

3. Inverse scattering by an inhomogeneous medium

3.1. Topological derivative of L^2 cost functionals

The illumination by an incident wave u_i of a given trial obstacle $D_\star$, characterized by an assumed contrast $q_\star$ such that $1 + q_\star \geqslant n_\star^2 > 0$ in $D_\star$ and $\overline{D}_\star = \mathrm{supp}(q_\star)$, generates the corresponding far-field pattern $v_\star^\infty$. Therefore, in order to quantify the discrepancy between $D_\star$ and the obstacle D to be identified, one may introduce the following type of least-squares cost functional $\mathcal{J}$ evaluating the misfit between far-field measurements v_{obs}^∞ of (9) and their trial counterpart $v_\star^\infty$:

$$\mathcal{J}(D_\star, q_\star) := \int_{\mathbb{S}} \frac{1}{2} \left| v_\star^\infty(\hat{x}) - v_{\mathrm{obs}}^\infty(\hat{x}) \right|^2 dS_{\hat{x}}. \tag{15}$$

One further assumes that the data v_{obs} featured in (15) consist of noise-free measurements on $\mathbb{S}$ of the acoustic field scattered by D, i.e. $v_{\mathrm{obs}}^\infty \equiv v^\infty$. The above functional assumes data from just one incident wave; multiple data may then be taken into account via finite sums or continuous superposition of functionals, as required.

Sampling methods are commonly investigated under the assumption that the full-aperture far-field data be available for *all* possible directions of incident plane waves, i.e. that the kernel $A(\hat{x}, \theta)$ of F be known from measurements for all $\hat{x}, \theta \in \mathbb{S}$, as these data uniquely determine the refraction index q (see e.g. theorem 6.26 in [1]). The cost functional of type (15) corresponding to this situation, denoted hereafter as $\mathcal{J}_{\mathbb{S}}$, is defined by

$$\mathcal{J}_{\mathbb{S}}(D_\star, q_\star) := \int_{\mathbb{S}} \int_{\mathbb{S}} \frac{1}{2} |A_\star(\hat{x}, \theta) - A(\hat{x}, \theta)|^2 \, dS_{\hat{x}} \, dS_\theta. \tag{16}$$

The case of a single incident wave of Herglotz type, i.e. of the form $u_i = Hg$ for some $g \in L^2(\mathbb{S})$, is also of interest, especially when g is selected on the basis of the full experimental information $A(\hat{x}, \theta)$. The corresponding cost functional of type (15), denoted by $\mathcal{J}[g]$ to emphasize its dependence on the Herglotz density g, is defined by

$$\mathcal{J}[g](D_\star, q_\star) := \int_{\mathbb{S}} \frac{1}{2} |Fg(\hat{x}) - F_\star g(\hat{x})|^2 \, dS_{\hat{x}}. \tag{17}$$

The remainder of this paper is mainly focused on studying the topological derivative of the cost functionals $\mathcal{J}_{\mathbb{S}}$ and $\mathcal{J}[g]$ as a means for the qualitative reconstruction of D.

Topological derivative. For a given *sampling* point $z \in \mathbb{R}^d$, let the trial obstacle be endowed with a uniform contrast $q_\star$ and geometrically defined by $D_\star = D_z^\varepsilon := z + \varepsilon\mathcal{D}$, where $\mathcal{D} \subset \mathbb{R}^d$ is a fixed open set containing the origin and with volume measure $|\mathcal{D}|$. The *topological derivative* $\mathcal{T}(z)$ of $\mathcal{J}$ at z is defined through the asymptotic expansion of $\mathcal{J}$ as $\varepsilon \to 0$:

$$\mathcal{J}(D_z^\varepsilon, q_\star) \underset{\varepsilon \to 0}{=} \mathcal{J}(\emptyset) + \eta(\varepsilon)\mathcal{T}(z) + o\big(\|v_{\varepsilon,z}^\infty\|_{L^2(\mathbb{S})}\big), \tag{18}$$

where $v_{\varepsilon,z}^\infty$ is the far-field pattern arising from the scattering of u_i by D_z^ε, $\eta(\varepsilon)$ defines the leading asymptotic behavior of $\mathcal{J}$ as $\varepsilon \to 0$ and $\mathcal{J}(\emptyset)$ is the value of $\mathcal{J}$ in the absence of any trial obstacle. Now, using the first-order Taylor expansion of $\mathcal{J}(D_z^\varepsilon, q_\star)$ with respect to $v_{\varepsilon,z}^\infty$, $\mathcal{T}(z)$ and $\eta(\varepsilon)$ are determined by the identification in the asymptotic equality (see e.g. [30]):

$$\eta(\varepsilon)\mathcal{T}(z) \underset{\varepsilon \to 0}{\sim} -\mathrm{Re}\left[\int_{\mathbb{S}} \overline{v^\infty(\hat{x})}\, v_{\varepsilon,z}^\infty(\hat{x})\, \mathrm{d}S_{\hat{x}}\right]. \tag{19}$$

The scattered field for the infinitesimal inclusion D_z^ε is known [34] to have the behavior

$$v_{\varepsilon,z}(x) = \varepsilon^d |\mathcal{D}| k^2 q_\star u_i(z)\Phi(x, z) + o(\varepsilon^d), \tag{20}$$

at any point $x \neq z$, implying that the corresponding far-field pattern reads

$$v_{\varepsilon,z}^\infty(\hat{x}) = \varepsilon^d |\mathcal{D}| k^2 q_\star u_i(z)h(z, -\hat{x}) + o(\varepsilon^d). \tag{21}$$

Considering an incident wave $u_i = Hg$ in (21) for some $g \in L^2(\mathbb{S})$, one therefore has $v_{\varepsilon,z}^\infty(\hat{x}) = F_z^\varepsilon g(\hat{x})$, with the far-field operator F_z^ε having the expansion

$$F_z^\varepsilon g(\hat{x}) = \varepsilon^d F_z^0 g(\hat{x}) + o(\varepsilon^d). \tag{22}$$

The operator F_z^0 therefore has (in the sense of definition (12)) a kernel A_z^0, given by

$$A_z^0(\hat{x}, \theta) = |\mathcal{D}| k^2 q_\star h(z, \theta)h(z, -\hat{x}) = |\mathcal{D}| k^2 q_\star \overline{\Phi_z^\infty(\theta)}\Phi_z^\infty(\hat{x}). \tag{23}$$

Replacing $v^\infty(\hat{x})$ by $Fg(\hat{x})$ and $v_{\varepsilon,z}^\infty(\hat{x})$ by $\varepsilon^d F_z^0 g(\hat{x}) + o(\varepsilon^d)$ in (19), the asymptotic behavior $\eta(\varepsilon)$ and the topological derivative $\mathcal{T}[g]$ of $\mathcal{J}[g]$ are found to be $\eta(\varepsilon) = \varepsilon^d$ and

$$\mathcal{T}[g](z) = -\mathrm{Re}\left[\int_{\mathbb{S}} \overline{Fg(\hat{x})}F_z^0 g(\hat{x})\, \mathrm{d}S_{\hat{x}}\right]. \tag{24}$$

Similarly, the same behavior $\eta(\varepsilon) = \varepsilon^d$ is found for $\mathcal{J}_{\mathbb{S}}$, with its topological derivative $\mathcal{T}_{\mathbb{S}}(z)$ obtained as

$$\mathcal{T}_{\mathbb{S}}(z) = -\mathrm{Re}\left[\int_{\mathbb{S}}\int_{\mathbb{S}} \overline{A(\hat{x}, \theta)}A_z^0(\hat{x}, \theta)\, \mathrm{d}S_{\hat{x}}\, \mathrm{d}S_\theta\right] \tag{25}$$

by replacing $v^\infty(\hat{x})$ by $A(\hat{x}, \theta)$ and $v_{\varepsilon,z}^\infty(\hat{x})$ by $\varepsilon^d A_z^0 g(\hat{x}, \theta) + o(\varepsilon^d)$ in (19), retaining the leading contribution as $\varepsilon \to 0$ and integrating the result over $\theta \in \mathbb{S}$. In addition, the following key relationships hold between topological derivatives and the far-field operator.

Proposition 1. *The topological derivatives* (24) *and* (25) *can be recast as follows in terms of the far-field operator F associated with the unknown scatterer (D, q):*

$$\mathcal{T}[g](z) = -|\mathcal{D}| k^2 q_\star \mathrm{Re}\big[\big(g, \Phi_z^\infty\big)_{L^2(\mathbb{S})}\big(\Phi_z^\infty, Fg\big)_{L^2(\mathbb{S})}\big], \tag{26a}$$

$$\mathcal{T}_{\mathbb{S}}(z) = -|\mathcal{D}| k^2 q_\star \mathrm{Re}\big[\big(\Phi_z^\infty, F\Phi_z^\infty\big)_{L^2(\mathbb{S})}\big]. \tag{26b}$$

Proof. Formula (26a) results from using $F_z^0 g(\hat{x}) = |\mathcal{D}| k^2 q_\star (g, \Phi_z^\infty)_{L^2(\mathbb{S})}\, \Phi_z^\infty(\hat{x})$ (by virtue of (23)) in (24) and treating the resulting integral over $\mathbb{S}$ as a scalar product in $L^2(\mathbb{S})$.

6

To establish (26*b*), one first uses definitions (23) of A_z^0 and invokes the reciprocity property $A(\hat{x}, \theta) = A(-\theta, -\hat{x})$ of F ([5], theorem 8.8), to obtain

$$\overline{A(\hat{x}, \theta)}A_z^0(\hat{x}, \theta') = -|\mathcal{D}|k^2 q_\star \overline{A(-\theta, -\hat{x})}\overline{h(z, -\hat{x})}h(z, \theta')$$
$$= -|\mathcal{D}|k^2 q_\star \overline{A(-\theta, -\hat{x})}\Phi_z^\infty(-\hat{x})\Phi_z^\infty(-\theta'),$$

for arbitrary $\theta, \theta' \in \mathbb{S}$. Equation (26*b*) then follows from integrating the result over $(\theta, \theta') \in \mathbb{S} \times \mathbb{S}$. $\qquad\qquad\qquad\qquad\qquad\qquad\qquad\qquad\qquad\qquad\qquad\qquad\qquad\square$

Remark 1. The leading asymptotics of the least-squares cost functionals considered in this study is remarkably expressed, as in (24) or (25), in terms of the conjugated (i.e. time reversed in the time domain) counterpart of the far-field pattern scattered by the unknown obstacle D. This observation leads directly to the key relations of proposition 1, which show the link between the topological derivative and the far-field operator.

3.2. Sign heuristic

The value $\mathcal{T}(z)$ quantifies the sensitivity of the featured cost functional $\mathcal{J}$ to the perturbation of the reference medium induced by the nucleation at $z \in \mathbb{R}^d$ of an infinitesimal obstacle with contrast $q_\star$. It is then natural to consider $z \mapsto \mathcal{T}(z)$ as a potential obstacle indicator function, as was previously done on several occasions (see [25–27] and the references therein). The heuristic underlying this usage is as follows: if $q_\star$ is of the same sign as q, then the sought object D (or the set thereof) is expected to be located at the sampling points z, at which $\mathcal{T}$ attains its most pronounced *negative* values, i.e. at which the introduction of a sufficiently small scatterer with a contrast of the same sign as that of D induces the most pronounced decrease of $\mathcal{J}$. Note that no smallness requirement for D is made in this approach, which is referred to hereafter as the *sign heuristic* of the topological derivative. Up to now, this sign heuristic lacks rigorous justification but is supported by many numerical experiments. This study aims at investigating the validity of such heuristic and determining conditions under which it has a mathematical justification, in the limited framework of the identification of obstacles characterized by refraction index perturbations using far-field data.

3.3. Born approximation

It is natural to begin by evaluating the validity of the topological derivative approach under the assumption of a weak-scatterer approximation for the sought object D before considering the more complex case of the full-scattering model (section 3.4). With reference to the Lippmann–Schwinger equation (6), this corresponds to situations where k, $|D|$, q are such that $\|ST_b\| \ll 1$. If $\|ST_b\| < 1$, equation (6) can be solved by fixed-point iterations. The first iterate, defined by $u_b = u_i$ in D and $v_b = ST_b u_i$ in $\mathbb{R}^d \setminus \bar{D}$, constitutes the Born approximation. The Born approximation is indicated by the subscript or superscript 'b' affixed to all relevant fields and operators. Moreover, one notes that, in view of (20), the probing infinitesimal trial obstacle also obeys the Born approximation.

Under the weak-scatterer approximation, the far-field operator has a known, and simple, factorization.

Lemma 2 ([10], section 4.3)**.** *The far-field operator under the Born approximation, denoted by F_b, is defined by (12) with the kernel A_b:*

$$A_b(\hat{x}, \theta) = \int_D k^2 q(y)\overline{h(y, \hat{x})}h(y, \theta)\, \mathrm{d}V_y, \qquad \hat{x}, \theta \in \mathbb{S}.$$

F_b is compact and (for real-valued contrast $q \in L^\infty(D)$) self-adjoint; as such, it has a complete orthonormal system with eigenvalues $\lambda_\ell^b \in \mathbb{R}$ and eigenfunctions $\Psi_\ell^b \in L^2(\mathbb{S})$. Moreover, it admits the factorization

$$F_b = H^\star T_b H,$$

where the operator $T_b : L^2(D) \to L^2(D)$ is defined by $T_b f = k^2 q f$ and with H, $H^\star$ as defined by (13a) and (13b).

Applying this factorization to (26a) and (26b) and using lemma 1 for every occurrence of $H\Phi_z^\infty$, one obtains more explicit expressions for the topological derivatives.

Proposition 2. *Under the Born approximation, the topological derivatives $\mathcal{T}^b[g]$ and $\mathcal{T}_\mathbb{S}^b$ are given (with the function ζ_0 as defined in lemma 1) by*

$$\mathcal{T}^b[g](z) = -|\mathcal{D}|k^2 q_\star \mathrm{Re}\left[(\Phi_z^\infty, g)_{L^2(\mathbb{S})}(T_b H g, H\Phi_z^\infty)_{L^2(D)}\right]$$

$$= -|\mathcal{D}|k^4 q_\star \mathrm{Re}\left[(\Phi_z^\infty, g)_{L^2(\mathbb{S})} \int_D q(y)\zeta_0(y-z)Hg(y)\,\mathrm{d}V_y\right], \quad (27a)$$

$$\mathcal{T}_\mathbb{S}^b(z) = -|\mathcal{D}|k^2 q_\star \left(H\Phi_z^\infty, T_b H\Phi_z^\infty\right)_{L^2(D)}$$

$$= -|\mathcal{D}|k^4 q_\star \int_D q(y)\zeta_0^2(y-z)\,\mathrm{d}V_y, \quad (27b)$$

where $g \in L^2(\mathbb{S})$ is arbitrary in (27a). Moreover, letting $g = \Psi_k^b$, where $\Psi_k^b \in L^2(\mathbb{S})$ is an eigenfunction of F_b for the eigenvalue $\lambda_k^b \in \mathbb{R}$, $\lambda_k^b \neq 0$, so that $F_b g = \lambda_k^b g$ (see lemma 2), one has

$$\mathcal{T}^b[\Psi_k^b](z) = -|\mathcal{D}|k^2 q_\star \lambda_k^b \left|\left(\Psi_k^b, \Phi_z^\infty\right)_{L^2(\mathbb{S})}\right|^2 \quad (28a)$$

$$= -|\mathcal{D}|k^2 q_\star (\lambda_k^b)^{-1} \left|\left(T_b H\Psi_k^b, H\Phi_z^\infty\right)_{L^2(D)}\right|^2. \quad (28b)$$

Proof. Formulae (27) are readily found by applying the factorization $F_b = H^\star T_b H$ to (26a) and (26b) and using lemma 1 for every occurrence of $H\Phi_z^\infty$. Next, (26a) with $g = \Psi_k^b$ reads

$$\mathcal{T}^b[g](z) = -|\mathcal{D}|k^2 q_\star \mathrm{Re}\left[(\Phi_z^\infty, \Psi_k^b)_{L^2(\mathbb{S})}(F_b \Psi_k^b, \Phi_z^\infty)_{L^2(\mathbb{S})}\right].$$

Formula (28a) then results from setting $F_b \Psi_k^b = \lambda_k^b \Psi_k^b$ in the second inner product, whereas formula (28b) is obtained by setting $\Psi_k^b = (\lambda_k^b)^{-1} F_b \Psi_k^b$ in the first inner product and using the factorization $F_b = H^\star T_b H$. □

Decay properties of the topological derivative. The topological derivatives as given in proposition 2 involves the function ζ_0 defined by (14), which has the well-known decay properties (see e.g. equations 10.7.8 and 10.52.3 in [33])

$$\zeta_0(x) = \mathcal{O}\left(|x|^{-1/2}\right)(\text{if } d = 2), \qquad \zeta_0(x) = \mathcal{O}\left(|x|^{-1}\right) \quad (\text{if } d = 3), \quad |x| \to +\infty. \quad (29)$$

As a result, $\mathcal{T}^b[g](z)$ and $\mathcal{T}_\mathbb{S}^b(z)$ decay away from D, as $\mathrm{dist}(z, D) \to \infty$, according to the following.

Proposition 3. *The topological derivatives $\mathcal{T}^b[g]$ (for any $g \in L^2(\mathbb{S})$) and $\mathcal{T}_\mathbb{S}^b$ have the following asymptotic behavior away from D:*

$$|\mathcal{T}^b[g](z)| = \mathcal{O}(\mathrm{dist}(z, D)^{(1-d)/2}), \qquad |\mathcal{T}_\mathbb{S}^b(z)| = \mathcal{O}(\mathrm{dist}(z, D)^{1-d}), \qquad |z| \to \infty. \quad (30)$$

Moreover, the above estimate for $\mathcal{T}^b[g]$ can be refined in two cases: (i) for any density $g \in C^0(\mathbb{S})$, one has

$$|\mathcal{T}^b[g](z)| = \mathcal{O}\big(|z|^{(1-d)/2}\mathrm{dist}(z,D)^{(1-d)/2}\big) \qquad |z| \to \infty, \tag{31}$$

and (ii) letting $g = \Psi_k^b$, where $\Psi_k^b \in L^2(\mathbb{S})$ is an eigenfunction of F_b for the eigenvalue $\lambda_k^b \in \mathbb{R}$, one has

$$|\mathcal{T}^b[g](z)| = \mathcal{O}(\mathrm{dist}(z,D)^{1-d}) \qquad |z| \to \infty. \tag{32}$$

Proof. Estimates (30) and (32) stem directly from invoking the Cauchy–Schwarz inequality and using (29) in (27*a*) and (27*b*) and (28*b*), respectively. Moreover, estimate (31) follows from

$$(\Phi_z^\infty, g)_{L^2(\mathbb{S})} = \int_{\mathbb{S}} \mathrm{e}^{-\mathrm{i}kz\cdot\hat{x}}\overline{g(\hat{x})}\,\mathrm{d}S_{\hat{x}} = \mathcal{O}(|z|^{(1-d)/2}),$$

which holds for any $g \in C^0(\mathbb{S})$ by virtue of known properties of oscillatory integrals (see e.g. [35], section 8.1). $\qquad\square$

The decay properties given by proposition 3 show that $z \mapsto |\mathcal{T}^b[g](z)|$ and $z \mapsto |\mathcal{T}_{\mathbb{S}}^b(z)|$ already permit a qualitative identification of D. The sign heuristic usually underlying the TD-based scatterer identification, which plays no role in proposition 3, is now studied.

Sign properties of the topological derivative.   First, in the case where q has a constant sign in D, it is clear from (27*b*) that

$$\mathrm{sign}(\mathcal{T}_{\mathbb{S}}^b(z)) = -\mathrm{sign}(q_\star q). \tag{33}$$

The topological derivative $\mathcal{T}_{\mathbb{S}}^b$, which is based on enough information for (D, q) to be exactly identifiable, is thus found to have both desired attributes of TD-based imaging, namely (i) the sharpest decay (among the variants considered) away from D, and (ii) a sign which is consistent with its heuristic meaning ($\mathcal{J}_{\mathbb{S}}$ decreases when a small trial scatterer such that $\mathrm{sign}(q_\star) = \mathrm{sign}(q)$ appears at z).

It does not appear that the sign of $\mathcal{T}^b[g]$ can be ascertained for arbitrary choices of g. However, for any eigenfunction $\Psi_k^b \in L^2(\mathbb{S})$ of F_b, one has $\mathrm{sign}(\lambda_k^b) = \mathrm{sign}(q)$ if $\mathrm{sign}(q)$ is constant in D due to $F_b = H^\star T_b H$ and the definition of T_b. Hence, if $g = \Psi_k^b$, the topological derivative $\mathcal{T}^b[\Psi_k^b]$, which exploits one single combination of the available measurement, has characteristics similar to $\mathcal{T}_{\mathbb{S}}^b$, namely is such that

$$\mathrm{sign}(\mathcal{T}^b[\Psi_k^b](z)) = -\mathrm{sign}(q_\star\lambda_k^b), \qquad |\mathcal{T}^b[\Psi_k^b](z)| = \mathcal{O}(\mathrm{dist}(z,D)^{1-d}) \;\; (|z| \to \infty). \tag{34}$$

Now, the more complex case where D is multiply connected (i.e. $\mathrm{supp}(q) = D = \cup_{m=1}^M D_m$) with q having constant sign in each connected component D_m, is considered. The topological derivative $\mathcal{T}_{\mathbb{S}}^b$ then satisfies the following corollary of propositions 2, 3.

Corollary 1. *Considering the case $d = 3$, let $\sigma_m := \mathrm{sign}(q|_{D_m})$, $\sigma_\star := \mathrm{sign}(q_\star)$, $\alpha := 16\pi^2 k^2 |\mathcal{D}|$ and define*

$$Q_m := \int_{D_m} q(y)\,\mathrm{d}V_y, \qquad \mathcal{I}_m(z) := -|\mathcal{D}|k^4 \int_{D_m} q_\star q(y)\zeta_0^2(z-y)\,\mathrm{d}V_y \quad (1 \leqslant m \leqslant M),$$

noting that $\mathrm{sign}(\mathcal{I}_m(z)) = -\sigma_\star\sigma_m$. Then, for any exterior sampling point $z_e \notin D$, one has

$$-\alpha \sum_{\sigma_\star\sigma_m=1} \frac{q_\star Q_m}{\mathrm{dist}(z,D_m)^2} \leqslant \mathcal{T}_{\mathbb{S}}^b(z_e) \leqslant -\alpha \sum_{\sigma_\star\sigma_m=-1} \frac{q_\star Q_m}{\mathrm{dist}(z,D_m)^2} \tag{35}$$

and for any interior point $z_i \in D_{m_0} \subset D$, where $m_0 \in \{1, \dots, M\}$, one has

$$\mathcal{I}_{m_0}(z_i) - \alpha \sum_{\substack{m \neq m_0 \\ \sigma_\star \sigma_m = 1}} \frac{q_\star Q_m}{\operatorname{dist}(z, D_m)^2} \leqslant \mathcal{T}_{\mathbb{S}}^b(z_i) \leqslant \mathcal{I}_{m_0}(z_i) - \alpha \sum_{\substack{m \neq m_0 \\ \sigma_\star \sigma_m = -1}} \frac{q_\star Q_m}{\operatorname{dist}(z, D_m)^2}. \tag{36}$$

Proof. Inserting the definition (14) of ζ_0 in (27b) and distinguishing between components D_m where $q_\star q_m$ is positive or negative, one has

$$\mathcal{T}_{\mathbb{S}}^b(z) = \alpha \left\{ - \sum_{\sigma_\star \sigma_m = 1} \int_{D_m} |q_\star q(y)| \frac{\sin^2(k|y-z|)}{|y-z|^2} \, dV_y \right.$$
$$\left. + \sum_{\sigma_\star \sigma_m = -1} \int_{D_m} |q_\star q(y)| \frac{\sin^2(k|y-z|)}{|y-z|^2} \, dV_y \right\} := \alpha(-S^+ + S^-).$$

If $z \notin D$, then for each $m = 1, \dots, M$

$$0 \leqslant \int_{D_m} |q_\star q(y)| \frac{\sin^2(k|y-z|)}{|y-z|^2} \, dV_y \leqslant \frac{|q_\star Q_m|}{\operatorname{dist}(z, D_m)^2},$$

and (35) follows from applying this inequality to derive separate upper bounds of the positive sums S^- and S^+. Note that the upper and lower bounds of this inequality are respectively positive and negative.

If $z \in D$, then there exists $m_0 \in \{1, \dots, M\}$ such that $z \in D_{m_0}$ and one similarly obtains

$$\mathcal{I}_{m_0}(z) - \alpha \sum_{\substack{m \neq m_0 \\ \sigma_\star \sigma_m = 1}} \frac{q_\star Q_m}{\operatorname{dist}(z, D_m)^2} \leqslant \mathcal{T}_{\mathbb{S}}^b(z) \leqslant \mathcal{I}_{m_0}(z) - \alpha \sum_{\substack{m \neq m_0 \\ \sigma_\star \sigma_m = -1}} \frac{q_\star Q_m}{\operatorname{dist}(z, D_m)^2}. \qquad \square$$

Remark 2. Proposition 3 and corollary 1 give a key justification to the heuristic of the topological derivative approach presented in section 3.1 under the Born approximation. Away from the scattering obstacle D, the expected decay of $\mathcal{T}_{\mathbb{S}}^b$ is $\mathcal{O}(\operatorname{dist}(z, D)^{1-d})$. Moreover, for a given m_0, if the probing scatterer $D_\star$ is qualitatively of same nature than D_{m_0} (i.e. if $\sigma_\star \sigma_{m_0} = 1$), then $\mathcal{T}_{\mathbb{S}}^b$ exhibits large negative values inside D_{m_0} provided that the effects of the remaining obstacle components D_m, $m \neq m_0$ can be neglected. In contrast, if $D_\star$ and a given D_{m_0} have opposite behaviors (i.e. $\sigma_\star \sigma_{m_0} = -1$), then pronounced positive values of $\mathcal{T}_{\mathbb{S}}^b$ occur inside D_{m_0}. This statement (that we do not formalize) is valid in the situations where the different geometrical components D_m are sufficiently far from each other or when their material contrasts are relatively low.

The inequalities (36) show that there exist configurations where the reconstruction of a given D_{m_0} can be skewed by the effects of the surrounding inhomogeneities, for example in terms of the sign of the topological derivative.

Remark 3. Corollary 1 does not have a simple counterpart for $d = 2$ because $J_0^2(x) \leqslant Cx^{-1}$ only in the limit $x \to \infty$, whereas $j_0^2(x) \leqslant Cx^{-2}$ for any $x > 0$.

Topological derivative in convolutional form.　　Let $f \star g$ denote the convolution product of functions $f, g \in L^2(\mathbb{R}^d)$, i.e.

$$[f \star g](x) = \int_{\mathbb{R}^d} f(y) g(x - y) \, dV_y.$$

By initial assumption, $q \in L^\infty(D)$ and has compact support $\bar{D}$; hence $q \in L^2(\mathbb{R}^d)$. The following proposition then follows by treating (27b) as a convolution integral.

Proposition 4. *Let the function* χ *be defined by* $\chi(x) = \zeta_0^2(x)$ *for all* $x \in \mathbb{R}^d$, *with* ζ_0 *as in lemma* 1*. The topological derivative* $\mathcal{T}_\mathbb{S}^b$ *is then given by*

$$\mathcal{T}_\mathbb{S}^b(z) = -|\mathcal{D}|k^4 q_\star [q \star \chi](z). \tag{37}$$

In formulation (37) of $\mathcal{T}_\mathbb{S}^b$, the convolution with the function χ acts as a filter on the material contrast function q, which has compact support. Therefore, the image provided by $\mathcal{T}_\mathbb{S}^b$ is expected to be a smoothed version of the actual object (D, q), with the value $\mathcal{T}_\mathbb{S}^b(z)$ at a given sampling point z related to the average of q over a neighborhood of z. This idea of geometrical filtering is analyzed next.

Remark 4. It is possible to find an asymptotic form of the right-hand side of (37) as $k \to \infty$. Within this type of approximation and owing to the known asymptotic behavior of $\zeta_0(z - y)$, the indicator function $\mathcal{T}_\mathbb{S}^b$ is expected to provide a sharper image of the sought obstacle. However, the relevance of this asymptotics remains constrained by the validity of the Born approximation (see discussion in section 5.3). In particular, in the short-wavelength regime, the contrast function q is restricted by (74) to very small values, which makes this type of approximation of very limited practical interest.

In order to obtain further insight into $\mathcal{T}_\mathbb{S}^b$ by exploiting its convolutional form (37), one introduces the Fourier transform of a function f as $\hat{f}$ defined by

$$\hat{f}(\xi) = \mathcal{F}[f](\xi) = \int_{\mathbb{R}^d} f(x) \, \mathrm{e}^{-2\pi \mathrm{i} x \cdot \xi} \, \mathrm{d}V_x.$$

The Fourier transform $\hat{\chi}$ of the radial function χ is also radial (see theorem IV.3.3 in [36]), and simple calculations with recourse to [37] show that

$$\hat{\chi}(\xi) = \frac{4\pi}{|\xi|} \frac{1}{(k^2 - \pi^2 |\xi|^2)^{1/2}} \qquad \left(\text{if } |\xi| < \frac{k}{\pi} \right), \quad \hat{\chi}(\xi) = 0 \quad \left(\text{if } |\xi| > \frac{k}{\pi} \right)$$

for $d = 2$, and

$$\hat{\chi}(\xi) = \frac{4\pi^3}{|\xi| k^2} \quad \left(\text{if } |\xi| < \frac{k}{\pi} \right), \qquad \hat{\chi}(\xi) = 0 \quad \left(\text{if } |\xi| > \frac{k}{\pi} \right)$$

for $d = 3$. From the identity (37), one obtains

$$\mathcal{T}_\mathbb{S}^b(z) = -|\mathcal{D}|k^4 q_\star [q \star \chi](z) = -|\mathcal{D}|k^4 q_\star \mathcal{F}^{-1}[\hat{q}(\xi)\hat{\chi}(\xi)](z). \tag{38}$$

Since $\hat{\chi}(\xi) = 0$ for $|\xi| > k/\pi$ for $d = 2$ or 3, equation (38) implies that spatial variations of q within a characteristic length scale smaller than $\lambda/2$, with $\lambda = 2\pi/k$, cannot be recovered. Hence, geometrical details of D on a scale smaller than the resolution limit $\lambda/2$ are filtered out in the reconstruction by the indicator function $\mathcal{T}_\mathbb{S}^b$.

In view of this resolution limit, it is natural to seek the transformation which, through deconvolution, will lead to the optimal reconstruction, in the L^2-norm sense, of the function q from $\mathcal{T}_\mathbb{S}^b$. To do so, let the functions Θ and Π be defined as follows in terms of their Fourier transforms:

$$\hat{\Theta}(\xi) = 1/\hat{\chi}(\xi) \quad \left(\text{if } 0 < |\xi| < \frac{k}{\pi} \right), \qquad \hat{\Theta}(\xi) = 0 \quad \left(\text{if } |\xi| > \frac{k}{\pi} \right) \tag{39a}$$

$$\hat{\Pi}(\xi) = 1 \quad \left(\text{if } |\xi| < \frac{k}{\pi} \right), \qquad \hat{\Pi}(\xi) = 0 \quad \left(\text{if } |\xi| > \frac{k}{\pi} \right). \tag{39b}$$

11

Using theorem IV.3.3 in [36], duality properties of the Fourier transform and equation 19.1.3 in [37], the function Π can be shown to be given by

$$\Pi(x) = \frac{k}{\pi} \frac{J_1(2k|x|)}{|x|} \quad \text{(if } d = 2\text{)}, \quad \Pi(x) = \frac{2k^2}{\pi^2} \frac{j_1(2k|x|)}{|x|} \quad \text{(if } d = 3\text{)}, \tag{40}$$

where J_1 is the Bessel function of the first kind and order 1 and j_1 its spherical counterpart. Then, the following corollary immediately follows from equation (38) and the definitions of functions Θ and Π.

Corollary 2. *With the functions Θ and Π defined by (39a) and (40), one has*

$$[\Theta \star \mathcal{T}_{\mathbb{S}}^b](z) = -|\mathcal{D}|k^4 q_\star [q \star \Pi](z).$$

The functions $\mathcal{T}_{\mathbb{S}}^b$ and $\Theta \star \mathcal{T}_{\mathbb{S}}^b$ both involve the convolution of the unknown contrast function q with a function of compact support $|\xi| \in [0; k/\pi]$. However, since in the Fourier domain one has

$$\mathcal{F}[\Theta \star \mathcal{T}_{\mathbb{S}}^b](\xi) = -|\mathcal{D}|k^4 q_\star \hat{q}(\xi) \quad \left(\text{if } |\xi| < \frac{k}{\pi}\right), \qquad \mathcal{F}\big[\Theta \star \mathcal{T}_{\mathbb{S}}^b\big](\xi) = 0 \quad \left(\text{if } |\xi| > \frac{k}{\pi}\right)$$

the convolution of $\mathcal{T}_{\mathbb{S}}^b$ with Θ allows to recover, up to the user-chosen factor $|\mathcal{D}|k^4 q_\star$, the Fourier transform of q for the spatial frequencies less than k/π. In fact, it is pointed out in [10] (p 93, after equation 4.21) that $\hat{q}$ is analytic (by virtue of $\hat{q}$ having compact support) and hence can in principle be recovered in all of $\mathbb{R}^d$ from its truncated version.

3.4. Full-scattering model

The topological derivative exploiting far-field measurements v^∞ of the scattered field is now formulated within the full-scattering model. In this framework, the following factorization holds for the far-field operator.

Lemma 3 ([10], theorem 4.5). *Let the far-field operator $F : L^2(\mathbb{S}) \to L^2(\mathbb{S})$ be defined by (12). Then*

$$F = H^\star T H \tag{41}$$

with operators H, $H^\star$ defined by (13a) and (13b), respectively. The operator $T : L^2(D) \to L^2(D)$ is defined by $T\varphi = (T_b^{-1} - S)^{-1}\varphi$ in terms of the operators $S : L^2(D) \to L^2(D)$ and $T_b : L^2(D) \to L^2(D)$ appearing in (6).

Proof. The proof follows [1, 10] and is presented for completeness. By superposition, for given $g \in L^2(\mathbb{S})$, Fg is the scattering far-field pattern arising from illuminating the inhomogeneity D by the incident wave $Hg \in L^2(D)$. By virtue of the Lippmann–Schwinger equation (6), the total field $u \in L^2(D)$ in D solves $(I - ST_b)u = Hg$ $(x \in D)$. By (8), the far-field pattern corresponding to u is then given by $H^\star T_b u$, i.e. by $H^\star T_b(I - ST_b)^{-1}Hg = H^\star(T_b^{-1} - S)^{-1}Hg$. Hence $F = H^\star(T_b^{-1} - S)^{-1}H$. $\square$

The topological derivatives and their decay properties are thus as follows.

Proposition 5. *Under the full-scattering model, the topological derivatives $\mathcal{T}[g]$ and $\mathcal{T}_{\mathbb{S}}$ are given by*

$$\mathcal{T}[g](z) = -|\mathcal{D}|k^2 q_\star \text{Re}\big[\big(\Phi_z^\infty, g\big)_{L^2(\mathbb{S})} \big(THg, H\Phi_z^\infty\big)_{L^2(D)}\big], \tag{42a}$$

$$\mathcal{T}_{\mathbb{S}}(z) = -|\mathcal{D}|k^2 q_\star \text{Re}\big[\big(H\Phi_z^\infty, TH\Phi_z^\infty\big)_{L^2(D)}\big]. \tag{42b}$$

Moreover, they decay with the distance dist(z, D) *according to*

$$|\mathcal{T}[g](z)| = \mathcal{O}(|z|^{(1-d)/2}\mathrm{dist}(z, D)^{(1-d)/2})$$
$$|\mathcal{T}_{\mathbb{S}}(z)| = \mathcal{O}(\mathrm{dist}(z, D)^{1-d}) \quad |z| \to \infty. \tag{43}$$

Proof. Formulas (42*a*) and (42*b*) result directly from applying lemma 3 to (26*a*) and (26*b*). Moreover, the decay properties (43) are identical to those obtained under the Born approximation and hold for the same reasons (they are not influenced by whether T, rather than T_b, is used in the factorization $F = H^\star T H$). $\qquad\square$

The far-field operator F is normal and compact [6]. As a consequence, there exists a complete set of orthonormal eigenfunctions $\Psi_\ell \in L^2(\mathbb{S})$ with corresponding eigenvalues $\lambda_\ell \in \mathbb{C}$ such that

$$Fg = \sum_{\ell=0}^{\infty} \lambda_\ell (g, \Psi_\ell)_{L^2(\mathbb{S})} \Psi_\ell. \tag{44}$$

This allows the following reformulations of $\mathcal{T}[g]$ and $\mathcal{T}_{\mathbb{S}}$.

Proposition 6. *The topological derivative* $\mathcal{T}_{\mathbb{S}}$ *is given in terms of the* $L^2(\mathbb{S})$*-orthonormal system* $(\lambda_\ell, \Psi_\ell)_{\ell \in \mathbb{N}}$ *of* F *by*

$$\mathcal{T}_{\mathbb{S}}(z) = -|\mathcal{D}|k^2 \sum_{\ell=0}^{\infty} q_\star \mathrm{Re}\,[\lambda_\ell] \left|\left(\Phi_z^\infty, \Psi_\ell\right)_{L^2(\mathbb{S})}\right|^2. \tag{45}$$

Moreover, letting $g = \Psi_k$ *for some* $k \in \mathbb{N}$*, the topological derivative* $\mathcal{T}[\Psi_k]$ *is given by*

$$\mathcal{T}[\Psi_k](z) = -|\mathcal{D}|k^2 q_\star \mathrm{Re}\big[\lambda_k^{-1}\big]\big|(TH\Psi_k, H\Phi_z^\infty)_{L^2(D)}\big|^2. \tag{46}$$

This in particular implies, by virtue of lemma 1 and (29), that

$$\mathcal{T}[\Psi_k](z) = \mathcal{O}(\mathrm{dist}(z, D)^{1-d}). \tag{47}$$

Proof. Reformulation (45) is obtained by using (44) into (42*b*), while (46) is established in the same way as (28*b*) with T_b replaced with T, taking advantage of the factorization (41). $\qquad\square$

The topological derivative $\mathcal{T}[g]$ can in fact easily be reformulated in terms of $(\Psi_\ell, \lambda_\ell)_{\ell \in \mathbb{N}}$ for arbitrary densities $g \in L^2(\mathbb{S})$; the resulting expression is not shown as it does not permit an additional general insight. Besides, the case of a single incident plane wave is summarized in the following remark.

Remark 5. The topological derivative for the case where D is probed using a single plane wave of incidence direction θ, denoted $\mathcal{T}[\theta](z)$, is obtained by replacing $Fg(\hat{x})$ with $A(\hat{x}, \theta)$ in (17), (24), (26*a*) and $(\Phi_z^\infty, g)_{L^2(\mathbb{S})}$ with $\Phi_z^\infty(\theta)$ in (26*a*). As a result, one obtains

$$\mathcal{T}[\theta](z) = -|\mathcal{D}|k^2 q_\star \mathrm{Re}\big[\Phi_z^\infty(\theta)H^\star TH\Phi_z^\infty(-\theta)\big]$$
$$= \mathcal{O}(\mathrm{dist}(z, D)^{(1-d)/2}) \qquad |z| \to \infty.$$

This case is easily generalized to measurements available for a finite number N of plane waves with incidence directions θ_n ($1 \leqslant n \leqslant N$), with the topological derivative at z then given by $\sum_{n=1}^{N} \mathcal{T}[\theta_n](z)$. Unsurprisingly (since the assumed available data is scarcer), the decay of $\mathcal{T}[\theta](z)$ away from D is less pronounced than that of $\mathcal{T}_{\mathbb{S}}(z)$ or $\mathcal{T}[\Psi_k](z)$. Moreover, $\mathrm{sign}(\mathcal{T}[\theta](z))$ cannot be ascertained from the above expression.

Propositions 5 and 6 address the decay of the topological derivative away from D, but not their sign properties; these are addressed next.

Sign properties of the topological derivative.   Determining the sign of the topological derivative is more difficult than in the case of the Born approximation. This has much to do with the fact that, F being normal but (unlike T_b) not self-adjoint, the eigenvalues λ_ℓ are complex-valued. They are in fact known [6, 38] to lie on the circle of the complex λ-plane defined by

$$k\gamma_d^2 |\lambda_\ell|^2 - \text{Im}[\lambda_\ell] = 0. \tag{48}$$

Equation (45) highlights the fact that the indicator function $z \mapsto \mathcal{T}_{\mathbb{S}}(z)$ defined in the topological derivative approach, based on an asymptotic expansion of the L^2 norm-based misfit function (16), reduces to the sum of the projections of the test function Φ_z^∞ onto the eigenvectors Ψ_ℓ of the far-field operator, weighted by the products $q_\star \text{Re}\,[\lambda_\ell]$ with the trial contrast $q_\star$ chosen *a priori*. Equation (45) shows that the sign of $\mathcal{T}_{\mathbb{S}}$ depends on the signs of $\text{Re}(\lambda_\ell)$, with $\mathcal{T}_{\mathbb{S}}(z)$ guaranteed to be negative if $\text{sign}[\text{Re}(\lambda_\ell)]$ is constant and equal to $\text{sign}(q_\star)$ for all $\ell \in \mathbb{N}$. Equation (48) implies that $-8\pi^2/k \leqslant \text{Re}(\lambda_\ell) \leqslant 8\pi^2/k$ and $\text{Im}(\lambda_\ell) \geqslant 0$ for any $\ell \in \mathbb{N}$, allowing one to readily characterize $\text{sign}[\text{Im}(\lambda_\ell)]$ but not $\text{sign}[\text{Re}(\lambda_\ell)]$ (whereas the latter sign was known in the Born approximation case). Indeed, the analytical example of section 3.5 will show that $\text{Re}(\lambda_\ell)$ can be either positive or negative for sufficiently high frequency and/or contrast, causing sign changes of $\mathcal{T}_{\mathbb{S}}(z)$ for $z \in D$. Likewise, the verification of the sign heuristic for $\mathcal{T}[\Psi_k]$ as given by (46) also requires $\text{sign}[\text{Re}(\lambda_k)] = \text{sign}(q_\star)$. However, this requirement can be satisfied in practice by selecting the pair (λ_k, Ψ_k) appropriately, since only one such pair is involved in (46).

It is nevertheless possible to extend the validity of the sign-characterization result (33) beyond the Born approximation, to a limited extent. To this end, assume that q has a constant sign over D and introduce the operator $\widetilde{S}: L^2(D) \to L^2(D)$ such that $\widetilde{S} = \text{sign}(q)T_b^{1/2}ST_b^{1/2}$, with the operator $T_b^{1/2} : L^2(D) \to L^2(D)$ defined by $T_b^{1/2}f = (k^2|q|)^{1/2}f$. Setting $\psi := T_b^{1/2}H\Phi_z^\infty \in L^2(D)$, and recalling that $T = (T_b^{-1} - S)^{-1}$, the topological derivative $\mathcal{T}_{\mathbb{S}}(z)$ can be recast from (42*b*) in the form

$$
\begin{aligned}
\mathcal{T}_{\mathbb{S}}(z) &= -|\mathcal{D}|k^2 q_\star \text{sign}(q)\text{Re}\big[\big(\psi, T_b^{-1/2}T T_b^{-1/2}\psi\big)_{L^2(D)}\big] \\
&= -|\mathcal{D}|k^2 q_\star \text{sign}(q)\text{Re}\big[(\psi, (I - \widetilde{S})^{-1}\psi)_{L^2(D)}\big].
\end{aligned}
$$

The following result then holds.

Proposition 7. *Assume that (i) q has a constant sign over D, and (ii) D, k and q are such that $\|\widetilde{S}\| < 1/2$, where $\|\widetilde{S}\| := \sup_{\|\phi\|_{L^2(D)}=1} \|\widetilde{S}\phi\|_{L^2(D)}$. Then*

$$\text{sign}(\mathcal{T}_{\mathbb{S}}(z)) = -\text{sign}(q_\star q).$$

Proof. Using the identity $(I - \widetilde{S})^{-1} = I + \widetilde{S}(I - \widetilde{S})^{-1}$, $\mathcal{T}_{\mathbb{S}}(z)$ is recast as

$$\mathcal{T}_{\mathbb{S}}(z) = -|\mathcal{D}|k^2 q_\star \text{sign}(q)\big(\|\psi\|_{L^2(D)}^2 + \text{Re}[(\psi, \widetilde{S}(I - \widetilde{S})^{-1}\psi)_{L^2(D)}]\big).$$

Moreover, one has $\|(I - \widetilde{S})^{-1}\| \leqslant 1/(1 - \|\widetilde{S}\|)$ whenever $\|\widetilde{S}\| < 1$. Applying the Cauchy–Schwarz inequality to $|(\psi, \widetilde{S}(I - \widetilde{S})^{-1}\psi)_{L^2(D)}|$, one thus obtains

$$|(\psi, \widetilde{S}(I - \widetilde{S})^{-1}\psi)_{L^2(D)}| \leqslant \frac{\|\widetilde{S}\|}{1 - \|\widetilde{S}\|}\|\psi\|_{L^2(D)}^2.$$

The condition $\|\widetilde{S}\| < 1/2$ therefore ensures that $|(\psi, \widetilde{S}(I - \widetilde{S})^{-1}\psi)_{L^2(D)}| < \|\psi\|_{L^2(D)}^2$ for any $\psi \in L^2(D)$. This in turn guarantees that $\|\psi\|_{L^2(D)}^2 + \text{Re}[(\psi, \widetilde{S}(I - \widetilde{S})^{-1}\psi)_{L^2(D)}] > 0$, which completes the proof. $\square$

Remark 6. The condition $\|\widetilde{S}\| < 1/2$ limits this sign-characterization result to scatterers of moderate strength, which are in particular within the applicability bounds of iterated Born (i.e. Neumann series) solution methods [39], while extending the corresponding result for the Born approximation case (for which $\|\widetilde{S}\| \ll 1$).

3.5. Analytical example: spherical scatterer in $\mathbb{R}^3$

Topological derivative.   To illustrate the foregoing developments, consider scattering by a *homogeneous* spherical obstacle D of unit radius and centered at the origin, so that $\partial D = \{x \in \mathbb{R}^3 : |x| = 1\}$. Assuming illumination by an incident plane wave $u_i = h(\cdot, \theta)$ propagating along the direction $\theta \in \mathbb{S}$, which can be expanded over the set of $L^2(\mathbb{S})$-orthonormal spherical harmonics $(Y_\ell^m)_{\ell \in \mathbb{N}, m \in \{-\ell, \dots, \ell\}}$ as

$$h(x, \theta) = \sum_{\ell=0}^{\infty} \sum_{m=-\ell}^{\ell} 4\pi \, \mathrm{i}^\ell j_\ell(k|x|) Y_\ell^m(\hat{x}) \overline{Y_\ell^m}(\theta) \tag{49}$$

by virtue of the Jacobi–Anger identity and the Legendre addition theorem (see e.g. equations 10.60.7 and 14.30.9 in [33]). The total field u in D and the scattered field v in $\mathbb{R}^3 \backslash D$ that together solve the forward scattering problem (1*a*)–(1*c*) can be similarly expanded as

$$u(x, \theta) = \sum_{\ell=0}^{\infty} \sum_{m=-\ell}^{\ell} u_\ell^m(\theta) j_\ell(nk|x|) Y_\ell^m(\hat{x}) \quad \text{for } x \in D, \theta \in \mathbb{S},$$

$$v(x, \theta) = \sum_{\ell=0}^{\infty} \sum_{m=-\ell}^{\ell} v_\ell^m(\theta) h_\ell(k|x|) Y_\ell^m(\hat{x}) \quad \text{for } x \in \mathbb{R}^3 \backslash D, \theta \in \mathbb{S},$$

where $n = \sqrt{1+q}$, j_ℓ and h_ℓ denote respectively the *p*th-order spherical Bessel and Hankel functions of the first kind. On using the transmission conditions $u = u_i + v$ and $n\partial_{|x|} u = \partial_{|x|}(u_i + v)$ on ∂D and the $L^2(\mathbb{S})$-orthonormality of spherical harmonics, the solution for v in $\mathbb{R}^d \backslash D$ is found to be given by

$$v(x, \theta) = 4\pi \sum_{\ell=0}^{\infty} \sum_{m=-\ell}^{\ell} \mathrm{i}^\ell \, \Lambda_\ell(q, k) \, h_\ell(k|x|) \, Y_\ell^m(\hat{x}) \overline{Y_\ell^m}(\theta), \tag{50}$$

with the coefficients $\Lambda_\ell(q, k)$ given by

$$\Lambda_\ell(q, k) = \frac{j_\ell(nk) j_\ell'(k) - n j_\ell'(nk) j_\ell(k)}{n j_\ell'(nk) h_\ell(k) - j_\ell(nk) h_\ell'(k)}$$

(f' denoting the derivative of f with respect to its argument). Note that $\Lambda_\ell(q, k)$ is non-singular, as the denominator $n j_\ell'(nk) h_\ell(k) - j_\ell(nk) h_\ell'(k)$ can be shown to be nonzero for any $k \in \mathbb{R}^+$ and $\ell \in \mathbb{N}$ (see e.g. [40]). Using equation (50) and theorem 2.15 of [5], the scattered [4] far-field pattern generated by a plane wave impinging on the unit penetrable ball centered at the origin is thus given by

$$v^\infty(\hat{x}, \theta) = \frac{16\pi^2}{\mathrm{i}k} \sum_{\ell=0}^{\infty} \Lambda_\ell(q, k) Y_\ell^m(\hat{x}) \overline{Y_\ell^m}(\theta).$$

Then, since the spherical harmonics Y_ℓ^m constitute an orthonormal system for $L^2(\mathbb{S})$, one concludes from definition (12) that the eigenvalues of the far-field operator F are given by

$$\lambda_\ell^m = \frac{16\pi^2}{\mathrm{i}k} \Lambda_\ell(q, k) \quad \text{for } \ell \in \mathbb{N}, m \in \{-\ell, \dots, \ell\} \tag{51}$$

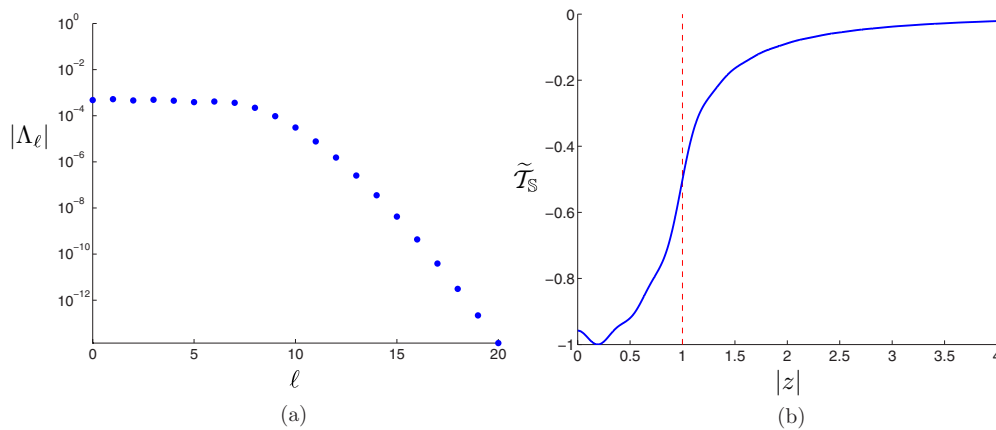**Figure 1.** Unit spherical obstacle with $q = 10^{-4}$ and $k = 10$. (a) Eigenvalues of F. (b) Radial plot of $\mathcal{T}_{\mathbb{S}}(z)$.

with the associated eigenfunctions $\Psi_\ell^m \equiv Y_\ell^m$, counting multiplicity. Note that equation (48) implies that Λ_ℓ satisfy $|\Lambda_\ell|^2 + \text{Re}[\Lambda_\ell] = 0$ for any $\ell \in \mathbb{N}$. The latter identity is also easily checked directly from definition (50) of Λ_ℓ and the fact that $j_\ell = \text{Re}[h_\ell]$. Finally, on applying the Jacobi–Anger expansion (49) to $\Phi_z^\infty(\hat{x}) = \overline{h(z, \hat{x})}$, using again the orthonormality of the Y_ℓ^m and invoking the identity $\sum_{m=-\ell}^{m=\ell} Y_\ell^m(\hat{z})\overline{Y_\ell^m(\hat{z})} = (2\ell + 1)/4\pi$ (a special case of the Legendre addition theorem), the topological derivative $\mathcal{T}_{\mathbb{S}}$ is found from (45) to be given by

$$\mathcal{T}_{\mathbb{S}}(z) = -64\pi^3 k\, q_\star |\mathcal{D}| \sum_{\ell=0}^\infty (2\ell + 1)\, \text{Im}[\Lambda_\ell(q, k)]\, j_\ell(k|z|)^2. \tag{52}$$

One can show from well-known limiting forms of the spherical Bessel functions (see e.g. [33], chapter 10) that the coefficients $\Lambda_\ell(q, k)$ admit the low-frequency expansion

$$\Lambda_\ell(q, k) = \mathrm{i}q \frac{k^{2\ell+3}}{(2\ell + 1)!!(2\ell + 3)!!}(1 + \mathcal{O}(k^2))$$

(where $n!! = 1 \times 3 \times \ldots n$ for any odd integer n) and the large-order expansion

$$\Lambda_\ell(q, k) = \mathrm{i}q \frac{k^3}{16\ell^3} \left(\frac{ek}{2\ell}\right)^{2\ell} (1 + \mathcal{O}(\ell^{-1})).$$

Both limiting cases are consistent with the sign heuristic of the topological derivative.

Results. This section provides some numerical results illustrating the behavior of the topological derivative (52) with $q_\star = q$. For the convenience of presentation, a normalization defined by

$$\widetilde{\mathcal{T}}(z) = (\max_z(|\mathcal{T}(z)|))^{-1}\mathcal{T}(z), \tag{53}$$

is applied to $\mathcal{T} = \mathcal{T}_{\mathbb{S}}$, and the rescaled version $\widetilde{\mathcal{T}}_{\mathbb{S}}$ is plotted for each example as a function of the distance $|z| \in [0; 4]$ to the center of D.

The first example assumes $q = 10^{-4}$ and $k = 10$, i.e. is well within the Born approximation. Figure 1(a) shows the sharp decrease of $|\Lambda_\ell|$ as ℓ increases, which justifies the approximate evaluation of the infinite series (52) at an appropriate truncation level ℓ_0 (the
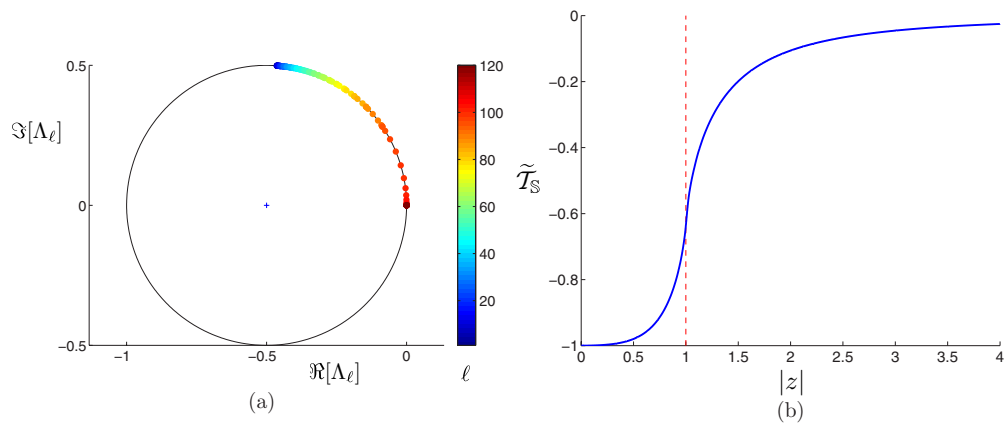
Figure 2. Identification of a unit spherical obstacle ($q = 1.5\,10^{-2}$, $k = 100$). (a) Eigenvalues of F in the complex plane. (b) Radial plot of $\mathcal{T}_{\mathbb{S}}(z)$.
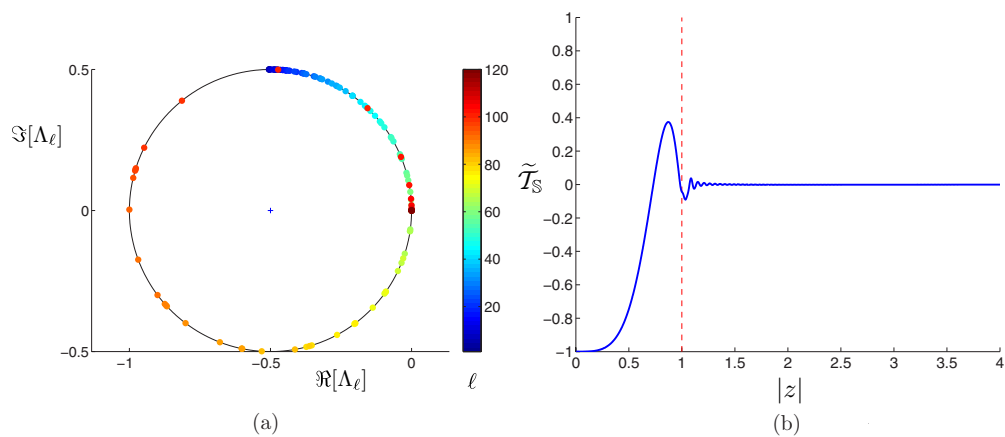

Figure 3. Identification of a unit spherical obstacle ($q = 8\,10^{-2}$, $k = 100$). (a) Eigenvalues of F in the complex plane. (b) Radial plot of $\mathcal{T}_{\mathbb{S}}(z)$.

examples of this section required $\ell_0 = 120$ at most). The largest negative values of $\mathcal{T}_{\mathbb{S}}$ occur inside D, as expected from the analysis of section 3.3 (figure 1(b)).

In the following two examples (figures 2 and 3), the parameters q and k are chosen so that the configurations correspond to limit cases in terms of the validity of the Born approximation. The eigenvalue sequences $\{\Lambda_\ell\}$, plotted in the complex plane on figures 2(a) and 3(a) (using colored dots, the color scale indicating the value of their order ℓ), are seen to accumulate at the origin in accordance with their large-order behavior, and also to lie on a circle as predicted by (48). However, the behavior of $\mathcal{T}_{\mathbb{S}}$ in these two cases is clearly different. In the first case, where $q = 1.5\,10^{-2} > 0$ (figure 2), one has $\text{Im}[\Lambda_\ell] > 0$ for all $\ell \in \mathbb{N}$, which ensures that $\widetilde{\mathcal{T}}_{\mathbb{S}}(z) < 0$ for all $z \in \mathbb{R}^3$ since $\text{sign}(q_\star q) = 1$; moreover, figure 2(b) shows that $\text{sign}(q_\star q) = 1$ attains pronounced negative values for $|z| < 1$, i.e. inside D. In the second case, where $q = 8\,10^{-2}$, figure 3(a) shows that the sequence $\{\text{Im}[\Lambda_\ell]\}$, and thus $\{\text{Re}[\lambda_\ell]\}$, has sign changes. Moreover, $\widetilde{\mathcal{T}}_{\mathbb{S}}(z)$, while being predominantly negative inside D (and hence acceptably consistent with the
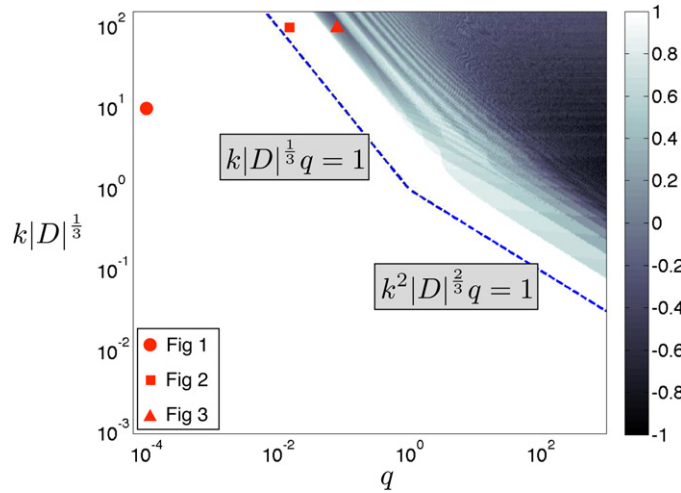
17

Figure 4. Average sign $\mathcal{S}(q, k)$ of the eigenvalues of the far-field operator.

original sign heuristic), also has sign changes. In both cases, $|\widetilde{\mathcal{T}}_{\mathbb{S}}(z)|$ decays as predicted away from D.

Validity of the sign heuristic. The decay of $|\mathcal{T}_{\mathbb{S}}(z)|$ away from D is characterized by (30) and (43), respectively, for the Born approximation and the full-scattering model, with the interpretation of the sign of $\mathcal{T}_{\mathbb{S}}(z)$ remaining an open question in the latter case when proposition 7 does not apply. Nonetheless, as emphasized by (45), the sign heuristic of the method is satisfied whenever $\mathrm{Re}(\lambda_\ell)$ all have the same sign, and may also be satisfied in other cases. If available measurements are sufficient for constructing the operator F, its eigenvalues are computable from the available data and their signs checkable. Moreover, as illustrated by the previously shown numerical results, satisfactory reconstructions are still achievable in cases where $\mathrm{sign}[\mathrm{Re}(\lambda_\ell)]$ is not constant (as in figure 3).

To investigate further the sign heuristic on the present analytical example, the average sign $\langle S \rangle$ defined as a function of q and k by

$$\langle S \rangle (q, k) = \frac{1}{\ell_{\max}} \sum_{\ell=0}^{\ell_{\max}} \mathrm{sign}(\mathrm{Im}[\Lambda_\ell(q, k)]) \tag{54}$$

with the truncation parameter $\ell_{\max}(q, k) < 200$ set such that $\mathrm{Im}[\Lambda_\ell(q, k)] < 10^{-20}$ for all $\ell > \ell_{\max}$, is computed. One has $-1 \leqslant \langle S \rangle (q, k) \leqslant 1$ by construction, with $\langle S \rangle (q, k) = 1$ indicating a perfect verification of the sign heuristic. The function $\langle S \rangle$ is plotted in figure 4, with the validity limits of the Born approximation in the high- and low-frequency regimes (as defined by (73) and (74)) indicated by dashed lines and the configurations corresponding to figures 1–3 indicated by symbols. This plot indicates that $\langle S \rangle (q, k) = 1$ in a parameter region outside that defined by proposition 7 (and hence also beyond the Born approximation), in which the validity of the sign heuristic is thus corroborated empirically.

3.6. Numerical examples in $\mathbb{R}^2$

In this section, numerical results corresponding to the identification of a set of homogeneous scattering obstacles (i.e q is piecewise-constant and $D = \mathrm{supp}(q - 1)$) embedded in $\mathbb{R}^2$
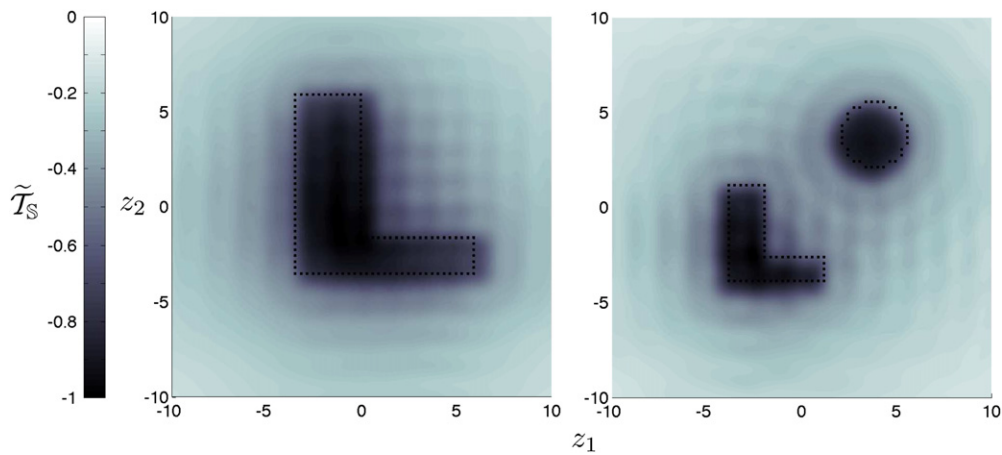
Figure 5. Identification of an inhomogeneous medium (dashed contour) with one (left) or two (right) components characterized by $q = 0.1$ and using $q_\star = 0.1$.
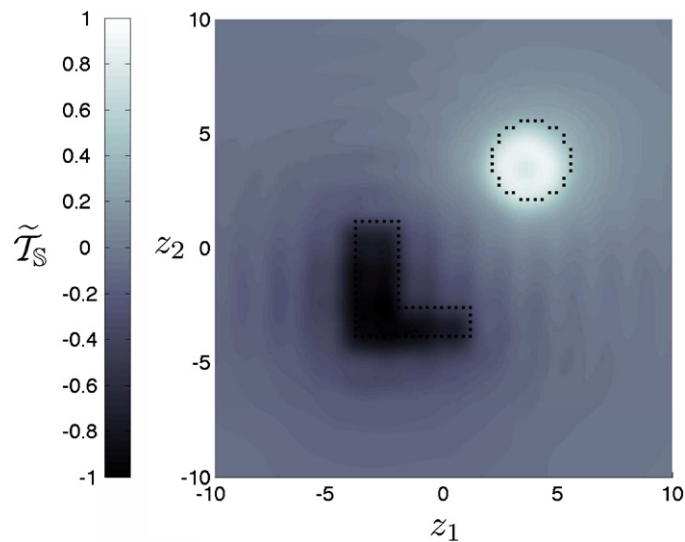

Figure 6. Identification of two scatterers respectively characterized by $q_1 = 0.1$ (lower left) and $q_2 = -0.1$ (upper right), using $q_\star = 0.1$.

are presented. The forward full-scattering model is implemented via a numerical solution of the Lippmann–Schwinger integral equation (6). The discretization method proposed in [41] is used, with the discretization length h adjusted to the wavelength according to $h = \lambda/10 = \pi/5k$. Given a set of $N = 60$ plane waves with $k = 2$ and equally spaced incident directions θ_j on $\mathbb{S}$ (with $\theta_j = (\cos(2\pi(j-1)/N), \sin(2\pi(j-1)/N))$ for $j = 1, \ldots, N$), synthetic measurements of the scattered far-field pattern (9) are generated for each configuration considered in order to compute the corresponding far-field operator (12). The topological derivative (42*b*) is then computed and its rescaled counterpart (53) is finally plotted (see figures 5–7) over the sampling region $z \in [-10; 10] \times [-10; 10]$.
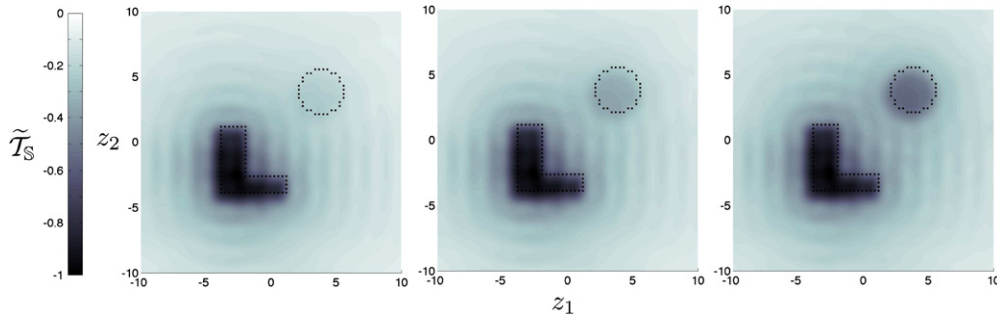
Figure 7. Identification of two scatterers characterized by $q_1 = 0.1$ (lower left) and $q_2 = \{0.01; 0.025; 0.05\}$ (upper right) and using $q_\star = 0.1$.

Figure 5 shows that satisfactory results are obtained for the identification of either a single L-shaped scatterer (left) or a set of two obstacles (one circular, one L-shaped), with the negative values of $\widetilde{\mathcal{T}}_{\mathbb{S}}(z)$ closest to -1 occurring in both cases in or near D. In particular, the two unknown obstacles are well resolved in figure 5 (right). On figure 6, the scatterer D considered has two homogeneous components characterized by $q_1 = 0.1$ and $q_2 = -0.1$, and $\mathcal{T}_{\mathbb{S}}$ is computed with $q_\star = q_1$. The locations and supports of the obstacles are well identified. Moreover, $\widetilde{\mathcal{T}}_{\mathbb{S}}(z)$ changes its sign from one object to the other as expected from the analysis of sections 3.3 and 3.4, with its most pronounced negative values occurring in the support of the scatterer for which $\text{sign}(q_\star q) = 1$. Finally, the identification of two objects with contrasts q_1, q_2 of the same sign is shown in figure 7 for three values $q_2/q_1 = 0.01$, 0.025, 0.05 of the contrast ratio (with $q_1 = 0.1$ in all cases). The results suggest that the best reconstructions are achieved when q_1 and q_2 have similar values.

4. Inverse scattering by point-like obstacles

4.1. Direct scattering problem and topological derivative

The analysis developed in section 3 can be carried over to small, point-like scatterers embedded in a homogeneous background medium. Such configurations define a simple, yet insightful framework for further comparison with some of the sampling methods mentioned in section 1. In this context, the topological derivative is closely related to a broader class of asymptotic methods [14] where geometrical information on small targets is recovered using asymptotic expansions of the forward solution. Such asymptotic analyses have been used in a number of studies for providing mathematical justifications to several imaging methodologies, in particular time reversal and DORT [42–44], MUSIC-type algorithms [45–47] and reverse-time migration [48].

4.2. Born approximation

Let $D = D^\delta$ denote a set of M point-like scatterers characterized by a common scaling size parameter $\delta > 0$, i.e. $D_m \equiv D_m^\delta := y_m + \delta \mathcal{D}_m$ with centers $y_m \in \mathbb{R}^d$, normalized shapes $\mathcal{D}_m \subset \mathbb{R}^d$ and real-valued constant contrasts q_m, $m = 1, \ldots, M$. Besides, let

$$a := \min_{1 \leqslant m < n \leqslant M} |y_m - y_n|$$

denote the minimal distance between the scatterers. Assuming illumination by the incident plane wave $u_i = h(\cdot, \theta)$ (see (3)), the corresponding scattered field reduces to sums of asymptotic formula (20) with z replaced by y_m and ε by δ, i.e.

$$v(x, \theta) = \sum_{m=1}^{M} Q_m k^2 u_i(y_m, \theta) \Phi(x, y_m) + o(\delta^d), \tag{55}$$

where $Q_m := \delta^d |\mathcal{D}_m| q_m$ is the reflectivity of the *m*th obstacle, while the kernel $A(\hat{x}, \theta)$ of the far-field operator is given by

$$A(\hat{x}, \theta) = A^0(\hat{x}, \theta) + o(\delta^d) = \sum_{m=1}^{M} A_m^0(\hat{x}, \theta) + o(\delta^d), \tag{56}$$

where, using (23), $A_m^0(\hat{x}, \theta)$ is given by $A_m^0(\hat{x}, \theta) = k^2 Q_m \overline{\Phi_{y_m}^\infty(\theta)} \Phi_{y_m}^\infty(\hat{x})$. In particular, the kernel $A^0(\hat{x}, \theta)$ thus defined is seen to be degenerate, of finite rank at most M. The leading-order small-scatterer asymptotic model (55) is a Born approximation in that it neglects the multiple scattering and the far field is explicitly given in terms of the incident field at the obstacle locations y_m.

For each point-like obstacle, define the Herglotz operator $H_m : L^2(\mathbb{S}) \to \mathbb{C}$, with adjoint $H_m^\star : \mathbb{C} \to L^2(\mathbb{S})$, by

$$H_m g := \int_{\mathbb{S}} h(y_m, \theta) g(\theta) \, \mathrm{d}S_\theta, \qquad H_m^\star f(\hat{x}) := h(y_m, -\hat{x}) f \tag{57}$$

and let $H : L^2(\mathbb{S}) \to \mathbb{C}^M$, with adjoint $H^\star : \mathbb{C}^M \to L^2(\mathbb{S})$, collect all H_m, i.e.

$$Hg := \{H_1 g, \dots, H_M g\}^{\mathrm{T}}, \qquad H^\star f(\hat{x}) = \sum_{m=1}^{M} H_m^\star f_m(\hat{x}) \quad (f = \{f_1, \dots, f_M\}^{\mathrm{T}} \in \mathbb{C}^M) \tag{58}$$

Then, using (56), the far-field operator (12) has the expansion and factorization

$$F = F^0 + o(\delta^d), \qquad F^0 = H^\star \boldsymbol{T}_b H \tag{59}$$

with $\boldsymbol{T}_b = k^2 \mathrm{diag}(Q_1, \dots, Q_M) \in \mathbb{C}^{M,M}$. Substituting (59) into (26*b*), the topological derivative $\mathcal{T}_\mathbb{S}$ is then found (using lemma 1 for the second equality) to be given by

$$\mathcal{T}_\mathbb{S}^b(z) = -k^2 q_\star |\mathcal{D}| \mathrm{Re} \left[(H\Phi_z^\infty)^\star \boldsymbol{T}_b H \Phi_z^\infty \right] = -k^4 q_\star |\mathcal{D}| \sum_{m=1}^{M} Q_m \zeta_0^2(z - y_m). \tag{60}$$

The magnitude $|\mathcal{T}_\mathbb{S}^b(z)|$ of $\mathcal{T}_\mathbb{S}^b$ hence (i) peaks at each location y_m and (ii) has a $\mathcal{O}(\mathrm{dist}(z, D^\delta)^{1-d})$ decay away from D^δ. In addition, similarly to section 3.3, one has $\mathrm{sign}[\mathcal{T}_\mathbb{S}^b(y_m)] = -\mathrm{sign}(q_\star Q_m)$ if either $M = 1$ or all reflectivities Q_m have the same sign; moreover, a counterpart to corollary 1 can easily be established from (60), to show that $\mathrm{sign}[\mathcal{T}_\mathbb{S}^b(y_m)] = -\mathrm{sign}(q_\star Q_m)$ also holds when the scatterers are well separated (i.e. for large enough ka). As a result, $\mathcal{T}_\mathbb{S}^b(z)$ permits a satisfactory identification of the locations y_m of a set of well-separated point-like scatterers.

In addition, the far-field operator F^0 is known (as a special case of [44], theorem 4.7) to be such that

$$F^0 h(y_m, \cdot) = 4\pi k^2 Q_m h(y_m, \cdot) + o((ka)^{-1}).$$

Moreover, the M functions $h(y_m, \cdot)$ are linearly independent ([44], proposition 13). Since the rank of F^0 is at most M, the eigensystem $(\lambda_\ell, \Psi_\ell)_{\ell \geqslant 1}$ of F^0 is approximately (in the sense of the above expansion) such that $\lambda_m := 4\pi k^2 Q_m$ are its only nonzero eigenvalues, with corresponding eigenfunctions $\Psi_m := h(y_m, \cdot)$. The topological derivative $\mathcal{T}^b[\Psi_m]$

corresponding to the illumination of D^δ with the single incident field $H\Psi_m$ is, by virtue of (28*a*) and using $(\Psi_m, \Phi_z^\infty)_{L^2(D)} = \zeta_0(y_m - z)$, given by

$$\mathcal{T}^b[\Psi_m](z) = -|\mathcal{D}|k^2 q_\star \lambda_m \big|(\Psi_m, \Phi_z^\infty)_{L^2(D)}\big|^2 = -4\pi|\mathcal{D}|k^4 q_\star Q_m \zeta_0^2(y_m - z). \tag{61}$$

Hence, $\mathcal{T}^b[\Psi_m](z)$ is seen to focus selectively on the obstacle D_m^δ. Moreover, $\mathcal{T}_{\mathbb{S}}^b(z)$ given by (60) is such that

$$4\pi\mathcal{T}_{\mathbb{S}}^b(z) = \sum_{m=1}^{M} \mathcal{T}^b[\Psi_m](z),$$

consistently with the fact that the $H\Psi_m$ are the only incident fields that produce nonzero far-field patterns when scattered by D^δ.

4.3. Multiple scattering using the Foldy–Lax model

Again assuming here illumination by the incident plane wave $u_i = h(\cdot, \theta)$, the Foldy–Lax model [49–52] accounts for multiple scattering in an approximate way, by assuming the scattered field $v(\cdot; \theta) = u - u_i(\cdot; \theta)$ to be given in terms of its Foldy–Lax approximation v^{FL}:

$$v(x, \theta) \approx v^{\text{FL}}(x, \theta), \qquad v^{\text{FL}}(x, \theta) := \sum_{m=1}^{M} Q_m k^2 u^{\text{FL}}(y_m, \theta)\Phi(x, y_m), \tag{62}$$

where Q_m are the obstacle reflectivities and $u^{\text{FL}}(y_m, \theta)$ are determined for given θ by enforcing the self-consistency conditions:

$$u^{\text{FL}}(y_m, \theta) = u_i(y_m, \theta) + \sum_{\substack{n=1 \\ n \neq m}}^{M} k^2 Q_n u^{\text{FL}}(y_n, \theta)\Phi(y_m, y_n), \qquad (m = 1, \ldots, M). \tag{63}$$

On introducing the matrix $\boldsymbol{S} \in \mathbb{C}^{M\times M}$ and the vector-valued functions $\boldsymbol{u}^i, \boldsymbol{u}^{\text{FL}}: L^2(\mathbb{S}) \to (L^2(\mathbb{S}))^M$ defined componentwise by

$$\begin{aligned} S_{mn} &= (1 - \delta_{mn})\Phi(y_m, y_n) \quad (m, n = 1, \ldots, M), \\ u_m^i(\theta) &= h(y_m, \theta), \quad u_m^{\text{FL}}(\theta) = u^{\text{FL}}(y_m, \theta) \quad (m = 1, \ldots, M), \end{aligned} \tag{64}$$

where δ_{nm} is the Kronecker symbol, the self-consistency conditions (63) for a given incidence direction $\theta \in \mathbb{S}$ written in matrix form reads $(\boldsymbol{I}_M - \boldsymbol{S}\boldsymbol{T}_b)\boldsymbol{u}^{\text{FL}}(\theta) = \boldsymbol{u}^i(\theta)$, with $\boldsymbol{I}_M$ denoting the $M \times M$ identity matrix and $\boldsymbol{T}_b = k^2\text{diag}(Q_1, \ldots, Q_M)$. With this notation, the far-field pattern associated with the Foldy–Lax model (62) is given by

$$v^{\text{FL},\infty}(\hat{x}, \theta) = H^\star[\boldsymbol{T}_b(\boldsymbol{I}_M - \boldsymbol{S}\boldsymbol{T}_b)^{-1}\boldsymbol{u}^i(\theta)](\hat{x}). \tag{65}$$

The following result then holds.

Lemma 4. *The far-field operator F^{FL}, defined by (12) with kernel $v^{\text{FL},\infty}$ given by (65), has the factorization*

$$F^{\text{FL}} = H^\star \boldsymbol{T}^{\text{FL}} H, \tag{66}$$

where the Herglotz operator H is defined by (58) and the matrix $\boldsymbol{T}^{\text{FL}} \in \mathbb{C}^{M\times M}$ is defined by $\boldsymbol{T}^{\text{FL}} = \boldsymbol{T}_b(\boldsymbol{I}_M - \boldsymbol{S}\boldsymbol{T}_b)^{-1} = (\boldsymbol{T}_b^{-1} - \boldsymbol{S})^{-1}$, with $\boldsymbol{T}_b = k^2\text{diag}(Q_1, \ldots, Q_M)$ and $\boldsymbol{S}$ given by (64).

Proof. Definition (58) of H implies that

$$Hg = \int_{\mathbb{S}} \boldsymbol{u}^i(\theta)g(\theta)\,\mathrm{d}S_\theta.$$

22

Evaluating $F^{\mathrm{FL}}g$ for some density $g \in L^2(\mathbb{S})$ using (65) and the above identity, one thus finds

$$F^{\mathrm{FL}}g(\hat{x}) = \int_{\mathbb{S}} v^{\mathrm{FL},\infty}(\hat{x},\theta)g(\theta)\,\mathrm{d}S_\theta = H^\star T^{\mathrm{FL}}Hg(\hat{x}).$$

$\square$

Substituting (66) into (26*b*), the topological derivative of (16) with data $v_{\mathrm{obs}}^\infty \equiv v^{\mathrm{FL},\infty}$ resulting from the Foldy–Lax model (62) is then found to be given by

$$\mathcal{T}_{\mathbb{S}}^{\mathrm{FL}}(z) = -k^2 q_\star |\mathcal{D}|\mathrm{Re}\left[(H\Phi_z^\infty)^\star T H\Phi_z^\infty\right]. \tag{67}$$

Assume that all obstacle reflectivities have the same sign, and let $\sigma = \mathrm{sign}(Q_1) = \cdots = \mathrm{sign}(Q_M)$. Define the matrices $\boldsymbol{T}_b^{1/2} = k\mathrm{diag}(\sqrt{|Q_1|},\ldots,\sqrt{|Q_M|}) \in \mathbb{C}^{M\times M}$, so that one has $\boldsymbol{T}_b = \sigma(\boldsymbol{T}_b^{1/2})^2$, and $\widetilde{\boldsymbol{S}} = \sigma \boldsymbol{T}_b^{1/2}\boldsymbol{S}\boldsymbol{T}_b^{1/2}$. Setting $\boldsymbol{\Psi}_z := \boldsymbol{T}_b^{1/2}H\Phi_z^\infty \in \mathbb{C}^M$, the topological derivative $\mathcal{T}_{\mathbb{S}}^{\mathrm{FL}}(z)$ can then be recast in the form

$$\mathcal{T}_{\mathbb{S}}^{\mathrm{FL}}(z) = -k^2 q_\star \sigma|\mathcal{D}|\mathrm{Re}\left[\boldsymbol{\Psi}_z^\star(\boldsymbol{I} - \widetilde{\boldsymbol{S}})^{-1}\boldsymbol{\Psi}_z\right].$$

Then, the following counterpart of proposition 7 holds.

Proposition 8. *If $Q_1,\ldots,Q_m$ are such that (i) $\mathrm{sign}(Q_1) = \cdots = \mathrm{sign}(Q_M) = \sigma$ and (ii) $\|\widetilde{\boldsymbol{S}}\| < 1/2$ (where $\|\cdot\|$ is the matrix norm induced by the 2-norm in $\mathbb{C}^M$), then*

$$\mathrm{sign}(\mathcal{T}_{\mathbb{S}}^{\mathrm{FL}}(z)) = -\sigma\,\mathrm{sign}(q_\star).$$

Proof. The proof is essentially identical to that of proposition 7, with operator $\widetilde{S}$ replaced with matrix $\widetilde{\boldsymbol{S}}$ and norm definitions adjusted accordingly. $\square$

4.4. The case of discrete far-field measurements

The developments of sections 4.2 and 4.3 can be repeated for the case where discrete far-field measurements at N angular locations $\hat{x} = \theta_n \in \mathbb{S}$ are available for a discrete set of incident plane waves propagating along the same directions θ_n, instead of continuous measurements for a continuous set of incidence directions. The main modifications consist in setting discrete counterparts of the Herglotz operator H and the far-field operator F. The former is the matrix $\boldsymbol{H} \in \mathbb{C}^{M\times N}$ such that $H_{mn} := h(y_m,\theta_n)$. The latter is the matrix $\boldsymbol{F}^b \in \mathbb{C}^{N\times N}$ (for the Born approximation) or $\boldsymbol{F}^{\mathrm{FL}} \in \mathbb{C}^{N\times N}$ (for the Foldy–Lax model), respectively defined by $F_{\ell n}^b = v^{b,\infty}(\theta_\ell,\theta_n)$ with $v^{b,\infty}$ given by (56) and $F_{\ell n}^{\mathrm{FL}} = v^{\mathrm{FL},\infty}(\theta_\ell,\theta_n)$ with $v^{\mathrm{FL},\infty}$ given by (65); $\boldsymbol{F}^b$ or $\boldsymbol{F}^{\mathrm{FL}}$ are known as multi-static response matrices. Cost functionals (16) and (17) are then accordingly replaced by appropriate finite sums. Defining the vector $\boldsymbol{\Phi}_z^\infty \in \mathbb{C}^N$ by $(\Phi_z^\infty)_n = \Phi_z^\infty(\theta_n) = h(z,-\theta_n)$, the counterparts of (60) and (61) are

$$\mathcal{T}_{\mathbb{S}}^b(z) = -|\mathcal{D}|k^2 q_\star(\boldsymbol{H}\boldsymbol{\Phi}_z^\infty)^{\mathrm{T}}\boldsymbol{T}_b\overline{\boldsymbol{H}\boldsymbol{\Phi}_z^\infty}, \qquad \mathcal{T}^b[\boldsymbol{\Psi}_m](z) = -|\mathcal{D}|k^2 q_\star\lambda_m\left|\boldsymbol{\Psi}_m^{\mathrm{T}}\overline{\boldsymbol{\Phi}_z^\infty}\right|^2 \tag{68}$$

(with $\lambda_m = k^2 Q_m\|\boldsymbol{\Phi}_{y_m}^\infty\|^2 \in \mathbb{R}$ and $\boldsymbol{\Psi}_m = \|\boldsymbol{\Phi}_{y_m}^\infty\|^{-1}\boldsymbol{\Phi}_{y_m}^\infty$) while the counterpart of (67) is

$$\mathcal{T}_{\mathbb{S}}^{\mathrm{FL}}(z) = -|\mathcal{D}|k^2 q_\star\mathrm{Re}\left[(\boldsymbol{H}\boldsymbol{\Phi}_z^\infty)^{\mathrm{T}}\overline{\boldsymbol{T}^{\mathrm{FL}}\boldsymbol{H}\boldsymbol{\Phi}_z^\infty}\right]. \tag{69}$$

Conclusions similar to those reached in sections 4.2 and 4.3 hold, including proposition 8, except for the fact that the rate of decay of $\boldsymbol{H}\boldsymbol{\Phi}_z^\infty$ as $\mathrm{dist}(z,D_M)$ is not known in general (i.e. for arbitrary finite sets of directions θ_n); it is expected to be slower than $\mathrm{dist}(z,D_M)^{-1}$ in general, and to decrease with N.
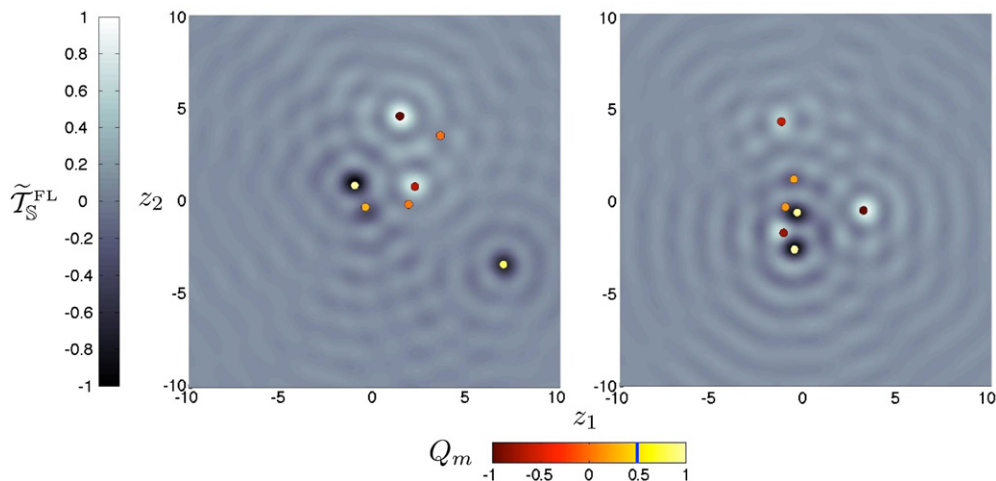
23

Figure 8. Identification of point-like obstacles using $\mathcal{T}_{\mathbb{S}}^{\mathrm{FL}}$ (with $q_\star = 0.5$).

4.5. Numerical examples in $\mathbb{R}^2$

In this section, numerical results concerning the identification of point-like scatterers in $\mathbb{R}^2$ are presented. The forward solution consists of the multi-static response matrix F^{FL} associated with the Foldy–Lax model (see section 4.4). A collection of $M = 7$ point obstacles, with randomly chosen locations $y_m \in \mathbb{R}^2$ and reflectivities $Q_m \in \mathbb{R}$ (the latter satisfying the constraint $Q_m \in [-1 + 10^{-3}, \, 1 - 10^{-3}]$), is illuminated using $N = 60$ incident plane waves with the wave number $k = 2$ and incidence directions θ_n equally spaced on the unit circle $\mathbb{S}$. The indicator function $\mathcal{T}_{\mathbb{S}}^{\mathrm{FL}}$ defined by (69) is then plotted, after rescaling according to (53), over the sampling region $z \in [-10; 10] \times [-10; 10]$.

Results on two such distributions of scatterers, indicated by small dots colored according to a scale indicating the value of their contrast Q_m, are presented in figures 8 and 9. The two figures differ by the choice of the contrast $q_\star$ of the probing inhomogeneity, which was set to $q_\star = 0.5$ for figure 8 and to $q_\star = -0.5$ for figure 9. The function $\mathcal{T}_{\mathbb{S}}^{\mathrm{FL}}$ reaches extremal values at the locations of the scatterers having largest absolute reflectivities $|Q_m|$, with the corresponding extrema being negative (respectively positive) at those locations where $q_\star Q_m > 0$ (respectively $q_\star Q_m < 0$) in accordance with the sign heuristic of the method.

5. Discussion

5.1. Far-field versus near-field settings

The chosen far-field configuration plays an important role in the results of this paper. In this context, the incident plane wave $h(z, \cdot)$ and the far-field pattern $\Phi_z^\infty = \overline{h(z, \cdot)}$ of $\Phi(z, \cdot)$ are, remarkably, mutually conjugated, leading to expression (26*b*) of $\mathcal{T}_{\mathbb{S}}$ where Φ_z^∞ appears on both sides of the $L^2(\mathbb{S})$ inner product. This in turn implies that $\mathcal{T}_{\mathbb{S}}$ is expressed in terms of a weighted sum of the squared moduli of the projections of Φ_z^∞ onto the eigenfunctions of F; see (45). In contrast, the near-field asymptotics (20) of $v_{\varepsilon,z}$ involves the fundamental solution $\Phi(\cdot, z)$, which has no particular relationship with an incident plane wave u_i. To extend the above-described symmetry in the formulation of $\mathcal{T}(z)$ to near-field cases, one has to consider
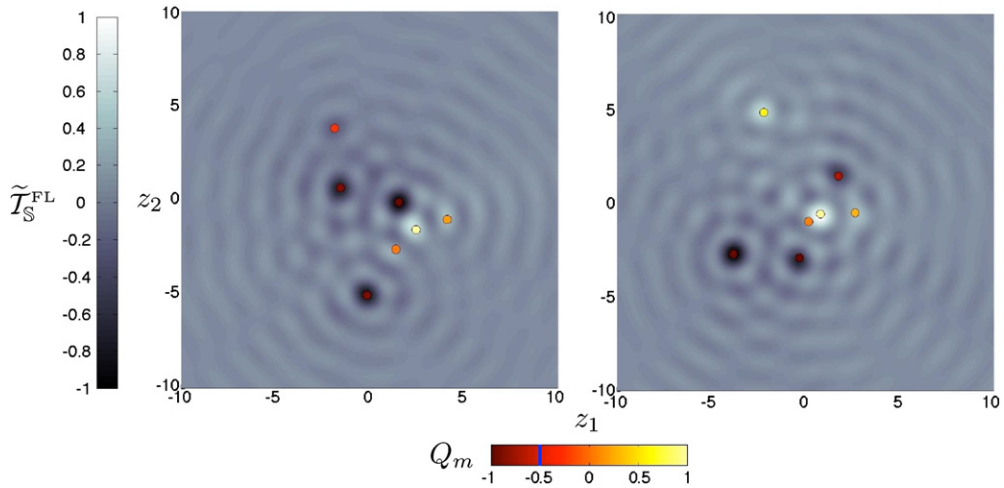
Figure 9. Identification of point-like obstacles using $\mathcal{T}_{\mathbb{S}}^{\mathrm{FL}}$ (with $q_\star = -0.5$).

illumination by point sources, rather than plane waves, since the incident field is then also expressed in terms of Φ.

5.2. Format of the cost functional

This study has concentrated on the topological derivative of cost functionals of least-squares type. The concept of topological derivative is however not restricted to this particular choice. Indeed, the concept of topological derivative originates from topological optimization, where numerous formats of objective functions are used. Considering for instance a generalization of the cost functional (15) where the misfit between the trial far-field $v_\star^\infty$ and its measured value v^∞ is evaluated using a distance function φ, the cost functional is now defined as

$$\mathcal{J}(D_\star, q_\star) := \int_{\mathbb{S}} \varphi(v_\star^\infty(\hat{x}) - v^\infty(\hat{x})) \, \mathrm{d}S_{\hat{x}}. \tag{70}$$

Then, advantage can be taken of an adjoint field-based formulation as it allows a generic closed-form expression of the corresponding topological derivative (see e.g. [31, 30]). Indeed, the asymptotic equality (19) associated with $\mathcal{J}$ defined by (70) takes the form

$$\eta(\varepsilon)\mathcal{T}(z) \underset{\varepsilon \to 0}{\sim} \mathrm{Re}\left[\int_{\mathbb{S}} \varphi'(-v^\infty(\hat{x})) v_{\varepsilon,z}^\infty(\hat{x}) \, \mathrm{d}S_{\hat{x}} \right],$$

(where the derivative φ' of the real-valued density $\varphi(z) = \tilde{\varphi}(\mathrm{Re}(z), \mathrm{Im}(z))$ is defined as $\varphi'(z) = [\partial_1 - \mathrm{i}\partial_2]\tilde{\varphi}(\mathrm{Re}(z), \mathrm{Im}(z)))$. Invoking the asymptotics (21) and defining the adjoint field $\hat{u}$ by

$$\hat{u}(z) := \int_{\mathbb{S}} \varphi'(-v^\infty(\hat{x})) h(z, -\hat{x}) \, \mathrm{d}S_{\hat{x}}. \tag{71}$$

($\hat{u}$ hence being a solution of the Helmholtz equation in $\mathbb{R}^d$), the topological derivative of (70) can finally be recast as

$$\mathcal{T}(z) = |\mathcal{D}| k^2 q_\star \, \mathrm{Re}[\hat{u}(z) \, u_i(z)]. \tag{72}$$

25

Applying this approach to generalizations of cost functionals $\mathcal{J}[g]$ and $\mathcal{J}_{\mathcal{S}}$ obtained by replacing $|\cdot|^2$ with $\varphi(\cdot)$ in (16) and (17), one similarly obtains

$$\mathcal{T}_{\mathbb{S}}(z) = |\mathcal{D}|k^2 q_\star \mathrm{Re}\left[\int_{\mathbb{S}} \hat{u}(z,\theta) h(z,\theta)\, \mathrm{d}S_\theta\right], \qquad \mathcal{T}[g](z) = |\mathcal{D}|k^2 q_\star \mathrm{Re}[\hat{u}(z)Hg(z)],$$

where $\hat{u}$ is defined by (71) with $v^\infty(\hat{x})$ respectively replaced by $Hg(\hat{x})$ and $A(\hat{x},\theta)$.

Expression (72) thus represents the generic formulation of the topological derivative of a cost functional of the form (70). Its usefulness comes from the fact that the information about the experiment, i.e. the measurements themselves and the format of the misfit function, are encapsulated in the definition of the adjoint field. It also helps in conferring flexibility to the concept of topological derivative in terms of (i) the nature and quantity of available measurements exploitable, and (ii) the available choices of cost functionals. In practice, numerical experiments on other, more complex problems [27] indicate that the number of sources and observations can be substantially reduced while inducing only moderate degradations on the reconstructions.

5.3. Validity of the Born approximation

Since the most comprehensive justification of the topological derivative for the scatterer identification was obtained under Born approximation conditions (sections 3.3 and 4.2), it is important to specify its domain of validity, which is dictated by the requirement $\|ST_b\| \ll 1$ (with S and T_b as defined in section 2). This issue is discussed in, e.g., section 8.10.1 of [53], where $\|ST_b\| \ll 1$ is translated into the following conditions on k, q, $|D|$ using dimensional analysis (with $|D|$ denoting the d-dimensional volume of $D \subset \mathbb{R}^d$):

$$k^2|D|^{\frac{2}{d}} \max_D |q| \ll 1, \tag{73}$$

in the low-frequency, long-wavelength limit (i.e. if $k|D|^{1/d} \ll 1$), and

$$k|D|^{\frac{1}{d}} \max_D |q| \ll 1. \tag{74}$$

In the high-frequency, short-wavelength limit (i.e. if $k|D|^{1/d} \gg 1$). The numerical results of section 3.5 are consistent with the above considerations. Since $k = 10$ (figure 1) or $k = 100$ (figures 2 and 3) and $|D| = 4\pi/3$, all three cases can be considered as short-wavelength situations. Given the respective values of q used, the Born approximation is reasonable in the first case, but not in the other two, as materialized in figure 4.

5.4. Relationships with other qualitative sampling methods

In this section, the commonalities of the topological derivative approach with some of the qualitative sampling methods among the most prominent examples mentioned in section 1 are discussed. The far-field operator (or its discrete counterpart, the multi-static response matrix), synthesizes the measurements and thus the available information on the unknown scattering object(s) that are accessible in a given excitation/observation setting. The central questions thus concern the extraction from F of these pieces of information, i.e. the reconstruction of the geometry D of the obstacle and the characterization of its material contrast q. The so-called sampling methods [2] for inverse scattering are based on the construction of indicator functions that depend on a sampling point z covering a domain of interest in $\mathbb{R}^d$, and which aim at providing only qualitative pieces of information on the scatterer(s) location and material parameters, but in a computationally efficient framework. These techniques depart from customary, and costlier, iterative minimization approaches, which aim at quantitative reconstructions. For an overall discussion about the specific features of the topological derivative approach, reference can be made to [27].

Time reversal and DORT. As discussed in [28], the topological derivative in the time-domain involves time reversal in that the adjoint solution is defined in terms of an excitation that involves time-reversed measurement residuals. For the same reason, the frequency-domain topological derivatives (24) or (25) involve the conjugated counterpart of the scattered field measurements.

Moreover, a more precise connection can be made between the topological derivative approach and the DORT method [20]. The latter aims at identifying M point-like scatterers by exploiting the eigensystem of the time-reversal operator $F^\star F$, which is known to be given (since F is normal) by $(|\lambda_\ell|^2, \Psi_\ell)_{\ell \in \mathbb{N}}$ (conventionally numbered so that $|\lambda_1| \geqslant |\lambda_2| \geqslant \ldots$) in terms of the eigensystem $(\lambda_\ell, \Psi_\ell)_{\ell \in \mathbb{N}}$ of F. More precisely, $\lambda_1, \ldots, \lambda_M$ are the only nonzero eigenvalues, and the incident field $u_i := H\Psi_m$ peaks at y_m, i.e. focuses on the mth scatterer (see [43, 44] for a mathematical justification).

The topological derivative $\mathcal{T}[\Psi_\ell]$ associated with the same incident fields $u_i := H\Psi_\ell$ is in fact found to have similar focusing properties for point-like as well as extended scatterers, and whether or not the Born approximation is used. Indeed, the magnitude of $\mathcal{T}[\Psi_\ell](z)$, given by (28*b*), (46), (61) according to the situation, consistently exhibits a $\mathcal{O}(\mathrm{dist}(z, D)^{1-d})$ decay away from D. This decay, observed for a single, selective probing wave, is (i) identical to that experienced by the topological derivative $|\mathcal{T}_\mathbb{S}(z)|$ combining all possible directions of probing incidence, and (ii) sharper than that of $|\mathcal{T}[\theta](z)|$ corresponding to illumination by a single (or finitely many) plane wave(s) (see remark 5).

MUSIC. The MUSIC algorithm has been originally introduced in inverse scattering problems to detect point-like scatterers satisfying the Born approximation (i.e. within the setting of section 4.2). It is based on the characterization

$$z \in \{y_1, \ldots, y_M\} \quad \Longleftrightarrow \quad \Phi_z^\infty \in \mathcal{R}(H^\star),$$

which, using that $\mathcal{R}(F^0 F^{0\star}) = \mathcal{R}(F^0) = \mathcal{R}(H^\star)$, leads to computing

$$\mathcal{I}_{\mathrm{MUSIC}}(z) := 1/\|P_\mathcal{N}\, \Phi_z^\infty\| \tag{75}$$

(with the projection $P_\mathcal{N} = I - P$ onto the noise subspace defined in terms of the projection P onto $\mathcal{R}(F^0 F^{0\star})$) and finding the locations $z = y_1, \ldots, y_M$ at which $\mathcal{I}_{\mathrm{MUSIC}}(z)$ has peaks.

The projection $P\Phi_z^\infty$ is found by means of a straightforward finite-dimensional least-squares minimization of $\|\Phi_z^\infty - H^\star \beta\|^2_{L^2(\mathbb{S})}$ with respect to $\beta \in \mathbb{C}^M$ (with H defined by (58)) to be given by

$$P\Phi_z^\infty(\hat{x}) = \left[H^\star G^{-1} H \Phi_z^\infty \right](\hat{x}) \quad (\hat{x} \in \mathbb{S}),$$

with

$$G \in \mathbb{R}^{M \times M}, \qquad G_{mn} = \int_\mathbb{S} h(y_m, \theta)\overline{h(y_n, \theta)}\, \mathrm{d}S_\theta = \zeta_0^2(y_m - y_n).$$

Noting that $H\Phi_z^\infty = \{\zeta_0(y_1 - z), \ldots, \zeta_0(y_M - z)\}^\mathrm{T} \in \mathbb{R}^M$, the above result implies that $\|P\Phi_z^\infty\|^2_{L^2(\mathbb{S})} = (H\Phi_z^\infty)^\mathrm{T} G^{-1} H\Phi_z^\infty$. For well-separated obstacles, i.e. $ka \gg 1$ with a as defined in section 4.2, one has $G = 4\pi I + \mathcal{O}((ka)^{-2})$, implying that $\|P\Phi_z^\infty\|^2_{L^2(\mathbb{S})} = (4\pi)^{-1}|H\Phi_z^\infty|^2 + \mathcal{O}((ka)^{-2})$, i.e. that $\|P\Phi_z^\infty\|_{L^2(\mathbb{S})}$ is approximately given by the 2-norm of $H\Phi_z^\infty$. One moreover observes that the topological derivative $\mathcal{T}_\mathbb{S}(z)$ for the same situation is given (up to a sign change and a multiplicative constant) by the weighted 2-norm $|H\Phi_z^\infty|_{T_b}$ of the same vector; see (60).

Comparing $\mathcal{T}_\mathbb{S}(z)$ and $\mathcal{I}_{\mathrm{MUSIC}}(z)$, the former is thus seen to exploit (a distorted version of) the projection of Φ_z^∞ onto the so-called signal subspace $\mathcal{R}(F)$, whereas the latter is based on the reciprocal of the projection of Φ_z^∞ onto the noise subspace.

Linear sampling and factorization methods.   The indicator functions $\mathcal{I}_{\mathrm{LSM}}(z)$ (for the linear sampling method), $\mathcal{I}_{\mathrm{FM}}(z)$ (for the factorization method) and $\mathcal{T}_{\mathbb{S}}$ are respectively given, in terms of the orthonormal system $(\lambda_\ell, \Psi_\ell)_{\ell \in \mathbb{N}}$ of F (see (44)), by

$$\mathcal{I}_{\mathrm{LSM}}(z) = \left[\sum_{\ell \in \mathbb{N}} \frac{|\lambda_\ell|}{|\lambda_\ell|^2 + \epsilon} \left| \left(\Phi_z^\infty, \Psi_\ell \right)_{L^2(\mathbb{S})} \right|^2 \right]^{-1},$$

$$\mathcal{I}_{\mathrm{FM}}(z) = \left[\sum_{\ell \in \mathbb{N}} \frac{1}{|\lambda_\ell|} \left| \left(\Phi_z^\infty, \Psi_\ell \right)_{L^2(\mathbb{S})} \right|^2 \right]^{-1},$$

$$\mathcal{T}_{\mathbb{S}}(z) = -|\mathcal{D}| k^2 q_\star \sum_{\ell \in \mathbb{N}} \mathrm{Re}\, [\lambda_\ell] \left| \left(\Phi_z^\infty, \Psi_\ell \right)_{L^2(\mathbb{S})} \right|^2$$

(with (45) repeated for convenience), where ϵ in $\mathcal{I}_{\mathrm{LSM}}(z)$ is a Tikhonov regularization parameter used in approximately solving for g_z the equation $F g_z = \Phi_z^\infty$ (which is ill-posed since F is compact), while $\mathcal{I}_{\mathrm{FM}}(z)$ expresses that $\Phi_z^\infty \in \mathcal{R}((F^\star F)^{1/4})$. All three approaches exploit the eigenvectors spanning the range of the far-field operator F, using Green's function Φ_z^∞ as an available test function.

   An issue of practical importance concerns the effect of measurement noise or background fluctuations on the available data F [27, 29]. The perturbation induced by the imperfect data to the evaluation of $\mathcal{T}_{\mathbb{S}}$ is linear in the data noise for the least-squares cost functional (15), and is more generally confined to the perturbation undergone by the adjoint solution $\hat{u}$ in expression (72), which is bilinear in $(u_i, \hat{u})$. On the other hand, both $\mathcal{I}_{\mathrm{LSM}}$ and $\mathcal{I}_{\mathrm{FM}}$ involve the reciprocals of the eigenvalues λ_ℓ, which makes their evaluation potentially sensitive to inaccuracies in the smallest eigenvalues. Moreover, the computation of $\mathcal{I}_{\mathrm{LSM}}(z)$ requires solving an ill-posed equation. Hence the evaluation of $\mathcal{I}_{\mathrm{LSM}}(z)$ or $\mathcal{I}_{\mathrm{FM}}(z)$ is expected to be more sensitive to noise in F than that of $\mathcal{T}_{\mathbb{S}}(z)$.

Orthogonality sampling method.   Owing to the relation (45), the topological derivative is conceptually comparable to the indicator function arising from the orthogonality sampling approach. The latter, recently introduced in [54] and discussed in [55], has been found to perform satisfactorily; its full mathematical justification is still open. No further insight into the topological derivative approach has so far been gained from this apparent analogy.

6. Conclusion

In this paper, the analysis of the topological derivative approach of inverse scattering problems by inhomogeneous acoustic media has been conducted to assess the reconstruction provided by the topological derivatives of L^2 cost functionals quantifying the misfit between measured and predicted far-field patterns. The particular structure of such misfit functions lead to imaging functionals in a form remarkably tractable in terms of analysis and comparison with other well-established qualitative and sampling methods. The sign heuristic of the method has been justified under either the Born approximation (i.e. extended inhomogeneities with weak contrast or well-separated point-like scatterers) or full-scattering models limited to moderately strong scatterers. While there is probably scope for enlarging the class of 'permitted' scatterers through a more-refined analysis, a justification of the heuristic reasoning underpinning the application of the topological derivative is not expected to be achievable for arbitrarily strong scatterers. Moreover, in view of numerical evidence in some strong-scatterer regimes, e.g. high-frequency configurations where the topological derivative is observed to highlight the obstacle boundary, there may be a need to define and justify another heuristic or interpretation suitable for such situations.

If the analysis that has been carried out in this paper applies to this, restricting yet widely used, definition of the cost functional, this formulation has enabled the shedding of new light on the mathematical foundations of the topological derivative approach of inverse scattering problems. One notes that the study [29] has also been conducted for a least-squares measurement misfit functional.

This study represents a step toward establishing a mathematical basis supporting the topological derivative for inverse scattering and understanding its links with other sampling approaches. Extensions of this work will address other types of inverse scattering problems, e.g. involving mass density contrasts, and the case of near-field measurements.

Acknowledgement

References

[1] Kirsch A 2011 *An Introduction to the Mathematical Theory of Inverse Problems* 2nd edn (Berlin: Springer)
[2] Cakoni F and Colton D 2006 *Qualitative Methods in Inverse Scattering Theory* (Berlin: Springer)
[3] Potthast R 2006 A survey on sampling and probe methods for inverse problems *Inverse Problems* **22** R1–R47
[4] Lax P and Phillips R S 1967 *Scattering Theory* (New York: Academic)
[5] Colton D and Kress R 1992 *Inverse Acoustic and Electromagnetic Scattering Theory* (Berlin: Springer)
[6] Colton D and Kress R 1995 Eigenvalues of the far field operator and inverse scattering theory *SIAM J. Math. Anal.* **26** 601–15
[7] Kirsch A 1998 Characterization of the shape of a scattering obstacle using the spectral data of the far field operator *Inverse Problems* **14** 1489–512
[8] Mast T D, Nachman A I and Waag R C 1997 Focusing and imaging using eigenfunctions of the scattering operator *J. Acoust. Soc. Am.* **102** 715–25
[9] Arens T and Lechleiter A 2009 The linear sampling method revisited *J. Integral Eqns Appl.* **21** 179–202
[10] Kirsch A and Grinberg N 2008 *The Factorization Method for Inverse Problems* (New York: Oxford University Press)
[11] Cheney M 2001 The linear sampling method and the MUSIC algorithm *Inverse Problems* **17** 591–5
[12] Kirsch A 2002 The MUSIC-algorithm and the factorization method in inverse scattering theory for inhomogeneous media *Inverse Problems* **18** 1025–40
[13] Devaney A J 2000 Super-resolution processing of multi-static data using time reversal and MUSIC www.ece.neu.edu/faculty/devaney/preprints/paper02n_00.pdf
[14] Ammari H and Kang H 2004 *Reconstruction of Small Inhomogeneities from Boundary Measurements* (*Lecture Notes in Mathematics* vol 1846) (Berlin: Springer)
[15] Devaney A J 2005 Time reversal imaging of obscured targets from multistatic data *IEEE Trans. Antennas Propag.* **53** 1600–10
[16] Cassereau D, Wu F and Fink M 1990 Limits of self-focusing using closed time-reversal cavities and mirrors—theory and experiment *IEEE Ultrasonics Symp.* vol 3 pp 1613–8
[17] Fink M 1992 Time reversal of ultrasonic fields—part I. Basic principles *IEEE Trans. Ultrason. Ferroelectr. Freq. Control* **39** 555–66
[18] Prada C, Thomas J L and Fink M 1995 The iterative time reversal process: analysis of the convergence *J. Acoust. Soc. Am.* **97** 62–71
[19] Borcea L, Papanicolaou G C, Tsogka C and Berrymann J G 2002 Imaging and time reversal in random media *Inverse Problems* **18** 1247–79
[20] Prada C and Fink M 1994 Eigenmodes of the time reversal operator: a solution to selective focusing in multiple target media *Wave Motion* **20** 151–63
[21] Prada C, Manneville S, Spoliansky D and Fink M 1996 Decomposition of the time reversal operator: application to detection and selective focusing on two scatterers *J. Acoust. Soc. Am.* **99** 2067–76
[22] Prada C, Tanter M and Fink M 1997 Flaw detection in solid with the DORT method *Proc. IEEE Ultrasonics Symp.* vol 1 pp 679–83
[23] Eschenauer H A, Kobelev V V and Schumacher A 1994 Bubble method for topology and shape optimization of structures *Struct. Optim.* **8** 42–51

29

[24] Jackowska-Strumillo L, Sokolowski J and Zochowski A 2003 Topological optimization and inverse problems *Comput. Assist. Mech. Eng. Sci.* **10** 163–76

[25] Bonnet M and Guzina B B 2004 Sounding of finite solid bodies by way of topological derivative *Int. J. Numer. Methods Eng.* **61** 2344–73

[26] Guzina B B and Chikichev I 2007 From imaging to material identification: a generalized concept of topological sensitivity *J. Mech. Phys. Solids* **55** 245–79

[27] Bellis C and Bonnet M 2010 A FEM-based topological sensitivity approach for fast qualitative identification of buried cavities from elastodynamic overdetermined boundary data *Int. J. Solids Struct.* **47** 1221–42

[28] Dominguez N, Gibiat V and Esquerré Y 2005 Time domain topological gradient and time reversal analogy: an inverse method for ultrasonic target detection *Wave Motion* **42** 31–52

[29] Ammari H, Garnier J, Jugnon V and Kang H 2012 Stability and resolution analysis for a topological derivative based imaging functional *SIAM J. Control Optim.* **50** 48–76

[30] Guzina B B and Bonnet M 2006 Small-inclusion asymptotic of misfit functionals for inverse problems in acoustics *Inverse Problems* **22** 1761–85

[31] Bonnet M 2008 Inverse acoustic scattering by small-obstacle expansion of a misfit function *Inverse Problems* **24** 035022

[32] Laurain A, Hintermüller M, Freiberger M and Scharfetter H 2013 Topological sensitivity analysis in fluorescence optical tomography *Inverse Problems* **29** 025003

[33] Olver F W J, Lozier D W, Boisvert R F and Clark C W (ed) 2010 *NIST Handbook of Mathematical Functions* (Cambridge: Cambridge University Press)

[34] Ammari H, Iakovleva E and Moskow S 2003 Recovery of small inhomogeneities from the scattering amplitude at a fixed frequency *SIAM J. Math. Anal.* **34** 882–90

[35] Stein E M 1993 *Harmonic Analysis: Real-Variable Methods, Orthogonality and Oscillatory Integrals* (Princeton NJ: Princeton University Press)

[36] Stein E M and Weiss G 1971 *Introduction to Fourier Analysis on Euclidean Spaces* (Princeton, NJ: Princeton University Press)

[37] Erdélyi A (ed) 1954 *Tables of Integral Transforms* (*Bateman Manuscript Project* vol 2) (New York: McGraw-Hill)

[38] Colton D and Kress R 1995 Eigenvalues of the far field operator for the Helmholtz equation in an absorbing medium *SIAM J. Appl. Math.* **55** 1724–35

[39] Kilgore K, Moskow S and Schotland J C 2012 Inverse Born series for scalar waves *J. Comput. Math.* **30** 601–14

[40] Guzina B B, Cakoni F and Bellis C 2010 On the multi-frequency obstacle reconstruction via the linear sampling method *Inverse Problems* **26** 125005

[41] Vainikko G 2000 Fast solvers of the Lippmann–Schwinger equation *Direct and Inverse Problems of Mathematical Physics* ed R P Gilbert, J Kajiwara and Y S Xu (Dordrecht: Kluwer Academic)

[42] Hazard C and Ramdani K 2004 Selective acoustic focusing using time-harmonic reversal mirrors *SIAM J. Appl. Math.* **64** 1057–76

[43] Pinçon B and Ramdani K 2007 Selective focusing on small scatterers in acoustic waveguides using time reversal mirrors *Inverse Problems* **23** 1–25

[44] Burkard C, Minut A and Ramdani K 2013 Far-field model for time reversal and application to selective focusing on small dielectric inhomogeneities *Inverse Problems Imaging* **7** 445–70

[45] Brühl M, Hanke M and Vogelius M S 2003 A direct impedance tomography algorithm for locating small inhomogeneities *Numer. Math.* **93** 635–54

[46] Ammari H, Iakovleva E, Lesselier D and Perrusson G 2007 MUSIC-type electromagnetic imaging of a collection of small three-dimensional inclusions *SIAM J. Sci. Comput.* **29** 674–709

[47] Iakovleva E, Gdoura S and Lesselier D 2007 Multi-static response matrix of a 3-d inclusion in a half space and MUSIC imaging *IEEE Trans. Antennas Propag.* **55** 2598–609

[48] Ammari H, Garnier J and Sølna K 2012 A statistical approach to optimal target detection and localization in the presence of noise *Waves Random Complex Media* **22** 40–65

[49] Foldy L L 1945 The multiple scattering of waves *Phys. Rev.* **67** 107–19

[50] Lax M 1951 Multiple scattering of waves *Rev. Mod. Phys.* **23** 287–310

[51] Devaney A J, Marengo E A and Gruber F K 2005 Time-reversal-based imaging and inverse scattering of multiply scattering point targets *J. Acoust. Soc. Am.* **118** 3129–38

[52] Challa D P and Sini M 2012 Inverse scattering by point-like scatterers in the Foldy regime *Inverse Problems* **28** 125006

[53] Chew W C 1995 *Waves and Fields in Inhomogeneous Media* (New York: IEEE)

[54] Potthast R 2010 A study on orthogonality sampling *Inverse Problems* **26** 074015

[55] Griesmaier R 2011 Multi-frequency orthogonality sampling for inverse obstacle scattering problems *Inverse Problems* **27** 085005